Synthesis of Phosphate-Crosslinked Starch Nanoparticles for Drug Delivery

by

Anand Lopez

A thesis

presented to the University of Waterloo

in fulfilment of the

thesis requirements for the degree of

Master of Science

in

Chemistry (Nanotechnology)

Waterloo, Ontario, Canada, 2017

Author's Declaration

I hereby declare that I am the sole author of this thesis. This is a true copy of the thesis, including any required final revisions, as accepted by my examiners. I understand that my thesis may be made electronically available to the public.

Abstract

Drug delivery agents for chemotherapy drugs have gained significant interest over the past few decades due to the need to localize the treatment to cancer cells. So far, polymeric micelles, liposomes, and carbon-based nanomaterials, among others, have shown great promise for this purpose. Starch nanoparticles have emerged as an avenue for drug delivery due to their low toxicity, biocompatibility and low cost. In this work, starch nanoparticles internally crosslinked by sodium trimetaphosphate (STMP) were prepared using a phase inversion emulsion process. From dynamic light scattering, transmission electron microscopy and environmental scanning electron microscopy, the particle size was determined to be 200-500 nm, regardless of STMP concentration used in the synthesis. ^{31}P NMR determined that a wide variety of organic phosphates were present, apart from the desired phosphodiester crosslinking. These included triphosphates, monophosphates and diphosphates. In addition, like typical charged nanogels, these nanoparticles retained significant amounts of water when dispersed in solution. This was related to the electrostatic repulsion between the chains within the nanoparticle. The presence of salt decreased the amount of water retention by screening of this electrostatic repulsion. The prepared nanoparticles were, in general, non-toxic to HeLa cancer cells. In addition, all prepared nanoparticles displayed a high drug loading, with a maximum seen with 30 mol% STMP. This loading was higher at pH 7.6 compared to lower pH. Drug release occurred more readily at lower pH. Finally, it was seen that exposure to typical cell culture environments induced significant release of drug compared to simple buffer environments.

Acknowledgements

I would like to thank my supervisor, Juewen Liu, for his unwavering support, productive discussion and mentorship over my graduate studies. In addition, I would like to thank my committee members, Dr. Scott Taylor and Dr. Michael Tam. I would like to especially thank Dr. Taylor for advice in interpreting NMR spectra. Special thanks are extended to my research group in Professor Liu's lab: Yibo, Biwu, Lingzi, Zijie, Zhicheng, Runjhun and past members (Jimmy and Feng) for their constant willingness to assist and provide support when necessary. Finally, I would like to thank the ECO-WIN collaboration team, including Dr. Jean Duhamel, Dr. Mario Gauthier and Dr. Rajinder Pal from the University of Waterloo and Niels Smeets and Michael Kuska from ECO for their advice and discussion at various points. Very special thanks are extended to Steven Bloembergen, the ECO project leader for my research. His support, very helpful discussion have proven critical to my research experience. Finally, I would like to thank Janet Venne for the NMR measurements on the nanoparticles.

Dedication

I dedicate this thesis to my family for their continued support and encouragement for all my endeavours.

Table of Contents

List of Figures

List of Tables

List of Abbreviations

AGU: Anhydroglucose units

BLNP: Biopolymer Latex Nanoparticles

BSA: Bovine Serum Albumin

CMC: Critical micelle concentration

CNT: Carbon nanotube

Cy3: Cyanine 3

DAPI: 4',6-diamidino-2-phenylindole

DLS: Dynamic light scattering

DMEM: Dulbecco's Modified Eagle Medium

DNA: Deoxyribonucleic acid

DOX: Doxorubicin

DS: Diclofenac sodium

EDC: 1-Ethyl-3-(3-dimethylaminopropyl)carbodiimide

EPR: Enhanced permeation and retention

ESEM: Environmental Scanning Electron Microscopy

FA: Folic acid

FBS: Fetal Bovine Serum

FDA: Food and Drug Authority

FITC: Fluorescein isothiocyanate

GPC: Gel permeation chromatography

HeLa: Henrietta Lacks

HEPES: (4-(2-hydroxyethyl)-1-piperazineethanesulfonic acid)

HLB: Hydrophile-lipophile balance

IB: Ibuprofen

ID: Indomethacin

MTT: (3-(4,5-dimethylthiazol-2-yl)-2,5-diphenyl tetrazolium bromide)

MUC1: Mucin 1

MW: Molecular weight

NHS: N-Hydroxysuccinimide

NMR: Nuclear magnetic resonance

NSAID: Non-steroidal anti-inflammatory drug

O/W: Oil-in-water emulsion

PBS: Phosphate-Buffered Saline

PCR: Polymerase chain reaction

PEG: Poly (ethylene) glycol

PIE: Phase inversion emulsion

PIT: Phase inversion temperature

PSMA: Prostate specific membrane antigen

PTK7: Protein tyrosine kinase 7

RNA: Ribonucleic acid

RPM: Revolutions-per-minute

SELEX: Systematic evolution of ligand by exponential enrichment

SNP: Starch nanoparticle

STMP: Sodium trimetaphosphate

STMP-SNP: Phosphate-crosslinked starch nanoparticles

STPP: Sodium tripolyphosphate

TEM: Transmission electron microscopy

TEMPO: (2,2,6,6-Tetramethylpiperidin-1-yl)oxyl

Tween 85: Polyoxyethylenesorbitan Trioleate

W/O: Water-in-oil emulsion

Chapter 1. Introduction

Cancer is responsible for millions of deaths worldwide each year. In 2012 alone, there were 14 million new diagnoses and 8 million deaths as a result of the disease.[1] Cancer is not simply one disease; it is a broad family of illnesses with one thing in common: the uncontrolled growth and proliferation of specific kinds of cells without apoptosis (or programmed cell death). Once this happens in a particular organ or tissue, the process continues. Eventually, the cells from that particular area may migrate to other organs and tissues, forming new tumors. This is known as metastasis and is the major reason why cancer is very difficult to treat.[1]

Along with surgery and radiation treatment, chemotherapy is widely used in the treatment of cancer. This involves using cytotoxic drugs to directly kill the cancer cells. Several of these drugs vary in their mechanism of action. For example, doxorubicin, one of the main drugs, intercalates with DNA and is especially toxic to rapidly dividing cells (such as cancer cells).[2] Docetaxel, on the other hand, disrupts the process of cell division (also known as mitosis).[3] Docetaxel is much more hydrophobic compared to doxorubicin. One of the major limiting factors is that these drugs are non-discriminating; they affect both healthy and diseased cells. This leads to several debilitating side effects and inherently limits the dose that could be taken by an individual.[1] In addition, many chemotherapeutics are carcinogenic and may induce their own cancers after continued use. There is therefore a need to localize chemotherapy to the site of action, sparing healthy cells. The drug must be protected to some degree until it is internalized into the cancer cell for immediate action.[4] Towards this end, an entire field of research has been established to develop nanoscale materials for drug containment and delivery.

1.1 Drug Delivery Vehicles

The idea of using designed vehicles to deliver drugs within the body has been investigated over several decades, with varying degrees of success.[5] The growth of nanotechnology has been a major driving force for developing vehicles. Liposomes were one of the first structures to be implemented for drug delivery.[6] Due to hydrophobic interactions of phospholipids in water and the cylindrical shape of the lipids, they self-assemble into a spherical bilayer structure. The small hydrophilic cavity is used for loading hydrophilic drugs. The first report of liposomes for drug delivery was in 1971, where Gregoriadis *et al*. successfully encapsulated an enzyme (an amyloglucosidase).[6] Since that time, several liposome-based drug delivery systems have been studied and a few have completed clinical trials.[7–9] One major issue of liposome-based drug delivery systems is their instability under various conditions of pH and salt concentration, and low loading efficiency as well as degradation by other molecules in the body.[10]

Block copolymers are polymers containing multiple covalently-lined segments, each with a different structure. A common type is that one of the blocks is hydrophobic, while in the other type, one of the blocks is hydrophilic. In water, above the critical micelle concentration (CMC), these block co-polymers self-assemble to form micelles and the hydrophobic tails aggregate together to form a spherical domain. Masayuki *et al*. were among the first to use block co-polymer based micelles to encapsulate an anticancer drug.[11] In this study, they entrapped the hydrophobic drug, Adriamycin, with polyethylene glycol (PEG)-b-poly(aspartic acid) and observed the performance *in vivo*. Similar cell toxicity was seen when the drug alone was used, but the side effects from the use of polymeric micelles in rats were less pronounced, implying that the drug delivery was successful. Several studies have been done since then in the synthesis

and application of polymeric micelles for drug delivery, and one of the major issues is its low encapsulation efficiency without modification.[12,13]

The synthesis and characterization of carbon nanotubes in the 1990s opened up a new avenue of research in nanotechnology in the form of carbon-based nanostructures.[14] Later, more novel morphologies were found, such as graphene and carbon nanotubes. One main advantage of using carbon nanomaterials is the exploitation of physisorption for drug loading. Since drug molecules tend to be aromatic, they can stack favourably (due to π-π interactions) with the aromatic groups on the carbon nanomaterial surface.[15] However, the potential for drug delivery was limited since these materials were not biocompatible and the toxicity was (and still is) under investigation.[16] Several strategies have been implemented to make these materials biocompatible, namely functionalizing a biocompatible polymer or introducing hydroxyl groups on its surface. For example, Liu *et al*. were among the first to make carbon nanotubes biocompatible by functionalizing the surface with PEG.[17] Exploiting the favourable π-π interactions, they were able to see a drug loading as high as 400% by weight (drug/CNT). Graphene (or more specifically, graphene oxide) has also demonstrated similar loading capabilities and applications in drug delivery.[18–20] Besides toxicity, other issues are the cost and scalability of the synthesis, which would not lend itself to mass production.[21]

Besides the three aforementioned systems, there are other nanoscale carriers currently under investigation such as metal nanoparticles,[22,23] gels,[24,25] and dendrimers.[26–29] The progression of vehicles for drug delivery over time is shown in Figure 1. There are advantages and disadvantages for each carrier which limits their use in a clinical setting. The main parameters for each delivery vehicle are the cost, scalability of production and the performance (*in vitro*, *in vivo* and clinical).[5] For newer systems, only preliminary research has been done and

several more years of work would be needed to demonstrate superior performance to current treatments.

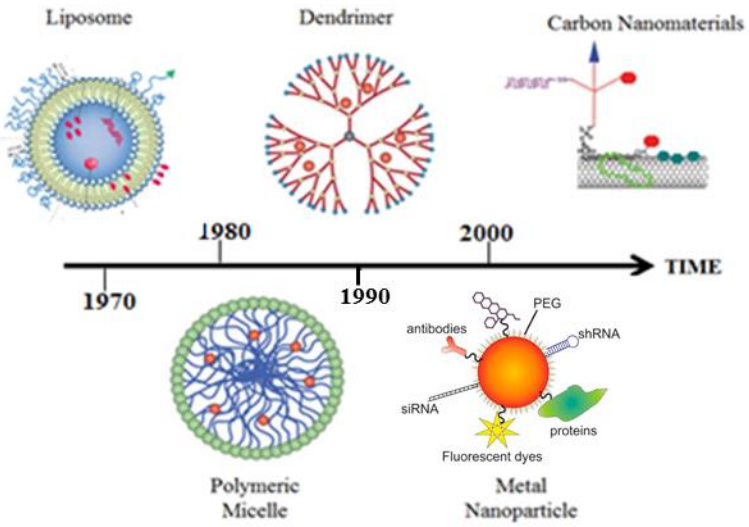

Figure 1. Progression of time for drug delivery vehicles.[9,30–32] This does not reflect necessarily when these materials were developed, but mainly when they were utilized for drug delivery. All images reproduced with permission.

1.2 Targeting Mechanisms

In the context of drug delivery, one key limitation for success is ensuring proper specificity; only carrying the drug to the diseased cells and leaving healthy cells unaffected. To this end, two approaches have been employed: passive targeting and active targeting.[33] For passive targeting, the nanocarrier loaded with drug would more likely accumulate in cancer cells than healthy cells due to abnormal growth and architecture coupled with a general lack of lymphatic drainage in the diseased cell. This is known as the enhanced permeability and retention (EPR) effect and is optimally seen in particles between 10 nm and 100 nm in size.[33] Once the particles aggregate within the tumor cells, their payload is ultimately released and the cancer cell dies.

Active targeting requires another step in the design of the nanocarrier: conjugation with a binding ligand. Most cancer cells have, on their surface, macromolecules (such as proteins) that will trigger internalization of an external agent within their cell walls through some binding event.[33] These macromolecules are known as receptors and the process by which the external agent is internalized is known as receptor-mediated endocytosis.[34] If a nanoparticle is conjugated with a ligand that binds to this receptor, the cell will internalize it. The receptors on the surface of a cancer cell will be present only for that type of cancer, allowing for selective targeting and sparing healthy cells. The ligand could be a protein, small molecule, or even DNA, as long as there is a significant binding event.

Strictly speaking, active targeting is preferable to passive targeting since the ultimate internalization would depend more on the functionalization of ligand on the surface (which could be known, and controlled) compared to passive targeting, where more emphasis is placed on the cellular architecture and drainage (which may not be optimal, and is difficult to find out).[33]

1.2.1 DNA Aptamers for Active Targeting

Unlike proteins, which have been studied extensively for the active targeting of cancer cell receptors, DNA/RNA aptamers have only recently been studied for this purpose.[35] This is because, until the late 1980s to early 1990s, there was no way to screen a large number of molecules for specific cell binding, isolate, and amplify the binding sequence.[36] This is now possible through a process known as Systematic Evolution of Ligand by Exponential Enrichment (SELEX). SELEX was used initially to find DNA strands to bind to proteins in yeast,[37] but has since been developed to detect various small molecules. To do this, it is necessary to start with a "DNA library"- a pool of random oligonucleotides (30-40 base pairs) flanked by two known

regions of nucleotides (between 15-20 base pairs).[38] The two known regions are primers for a process known as polymerase chain reaction (PCR). PCR amplifies specific DNA sequences using an enzyme (usually the *Thermus aquaticus* polymerase) and thermal cycling from a few copies to thousands or even millions.[39] The DNA library is incubated with the target molecule, and only oligonucleotides which have a certain affinity for the target (which are considered aptamer candidates) will bind. The unbound strands are separated and the bound strands are amplified using PCR. The amplified strands are then placed back into an environment containing the target and another round of selection is performed (with a selection pressure of reduced incubation time or target concentration).[38] This process is repeated several times until suitable DNA aptamers are found. Besides small molecules, DNA aptamers have been found that can bind to small molecules, metal ions, proteins, and even viruses.[40–42] More recently, SELEX has been found to work for whole cells and is known as cell-SELEX.[43–45] Most often, after finding the sequences that bind to the target cell, another step is added where a negative cell (i.e. a cell that is different to the target cell) is introduced into the selection.[44] To tune the selectivity, those sequences that bind to the non-cancerous cells are removed from subsequent amplification and optimization process.

There are several aptamers which have been found from cell-SELEX that have demonstrated specificity and high affinity for certain cancer cell lines.[46] Some of these aptamers are summarized in Table 1. These aptamers are classed according which receptors they bind to, and not according to the cancer cells themselves. This is because many cancer cell lines may have similar receptors on their surface and would internalize the DNA aptamer in the same way.

Table 1. Selected aptamers developed by cell-SELEX

Aptamer	Target	Reference
AS1411	Nucleolin	[46,47]
sgc8c	Protein Tyrosine Kinase 7 (PTK7)	[46,48]
5TR1	Mucin 1 (MUC1)	[46,49]
A10	Prostate-Specific Membrane Antigen (PSMA)	[46,50]
S11e	Unknown (specific to A549 lung cancer cells)	[51,52]

1.3 Starch as a Drug Delivery Vehicle

Starch (or more specifically, starch nanoparticles) has emerged as a new drug delivery vehicle in recent years since its chemistry is very well studied, its behaviour is predictable and it is very biocompatible.[53–55] Apart from being a carbohydrate that is widely found in many plant-based foods, bulk starch has found some applications in industry. For example, starch can be used to make various sugars (such as glucose and dextrose) which are used as sweeteners in the beverage industry.[56] Acid-modified starches (or hydrolysed starches) are used to lower the viscosity of the paste after cooking and are typically used in textiles.[57] As it is used so extensively in food industries, starch is FDA-approved for a variety of applications. A comparison of drug delivery vehicles in terms of various necessary parameters are shown in Table 2. These parameters often determine whether a certain drug delivery vehicle is viable and none of these are necessarily more important than the other.

Table 2. A comparison of various drug delivery agents and their properties.

Vehicle	Cost	Encapsulation Efficiency	Stability	Scalability	Toxicity	Reference
Liposomes	Low	Low	Low	High	Low	[10,58,59]
Polymeric Micelles	Variable	Low	Low	High	Low	[60,61]
Carbon Nano-materials	High	High	High	Low	Unknown	[16,17,62,63]
Dendrimers	High	Variable	High	Low	High	[64–66]
Starch Nano-particles	Low	Moderate	High	High	Low	[54,67,68]

1.4 Primary and Secondary Starch Structure

Starch is a polysaccharide derived from plants and is composed of two different polymers: amylose and amylopectin. The structures of these two polymers are shown in Figure 2. Amylose is simply a linear chain of glucose molecules linked together by a glycosidic bond, whereas amylopectin is significantly more branched. A glycosidic bond is one that occurs in carbohydrates where the 1-carbon of one glucose unit is linked to an anomeric carbon of another glucose unit. In the context of starch, glucose molecules are linked from the 1-carbon to the 4-carbon (called a α (1→4) glycosidic bond).[69] For amylopectin, branching takes place with a α(1→6) glycosidic bond, apart from the regular α (1→4) linkages.[70] The ratio of these two polymers in the overall starch structure depends significantly on the source of the starch. For example, starch derived from corn contains 27% amylose and 73% amylopectin, whereas potato starch is composed of 20% amylose and 80% amylopectin.[69]

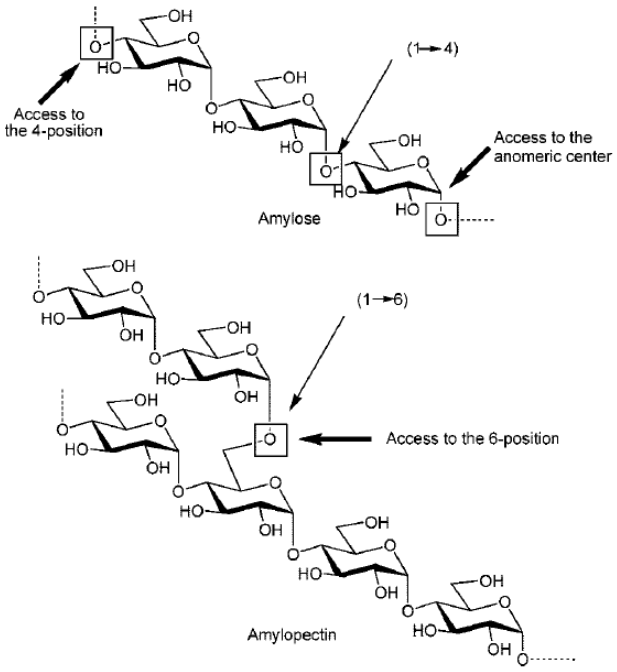

Figure 2. A comparison of (A) amylose and (B) amylopectin.[71] Amylose is a linear chain of glucose and can self-assemble into a helical structure. Amylopectin is a highly branched macromolecule where glycosidic bonds occur at the 6 carbon. Reproduced with permission.

1.5 Granular (Bulk) Starch

Starch is not soluble in water at room temperature and in fact, behaves like a suspension. This is because starch exists as granules that are typically several tens of microns in size.[69] The internal structure of these granules can be quite complicated as shown in Figure 3. Models could be used to gain an idea of the arrangement of amylopectin and amylose within the starch granule. In general, there is a centralized region known as the hilium, with concentric rings of alternating amorphous and crystalline regions around it.[72] Interestingly, while only amylose is capable of crystallization, crystalline regions in starch granules mainly consist of amylopectin (which, by itself, is not capable of crystallization). These crystalline domains stem from the oligosaccharide branches from the amylopectin with a chain length of approximately 23 glucose units and are

responsible for the crystalline "rings" within the granule.[73] The amorphous region consists of the branching points of amylopectin with interspersed amylose. Water molecules are not able to penetrate these highly ordered structures at room temperature. However, if heated above a certain temperature while mixed with water, the water molecules are able to penetrate the starch granules, causing them to swell.[69] Eventually, after heating for a certain amount of time the granules rupture, break apart, dissolve and release amylose and amylopectin chains. The amylose chains align to form a network, resulting in a significant increase in viscosity.[74] At this point, the water molecules act as a plasticizer for this crosslinked network and the starch is considered to be "dissolved". This entire process of starch gelatinization in water is known as cooking and is one of the main reactions performed to make starch soluble. It should be noted that this gelatinization can occur almost spontaneously in alkaline conditions (more specifically, pH>10) without significant heating due to increased rate of hydration of the granules.[69]

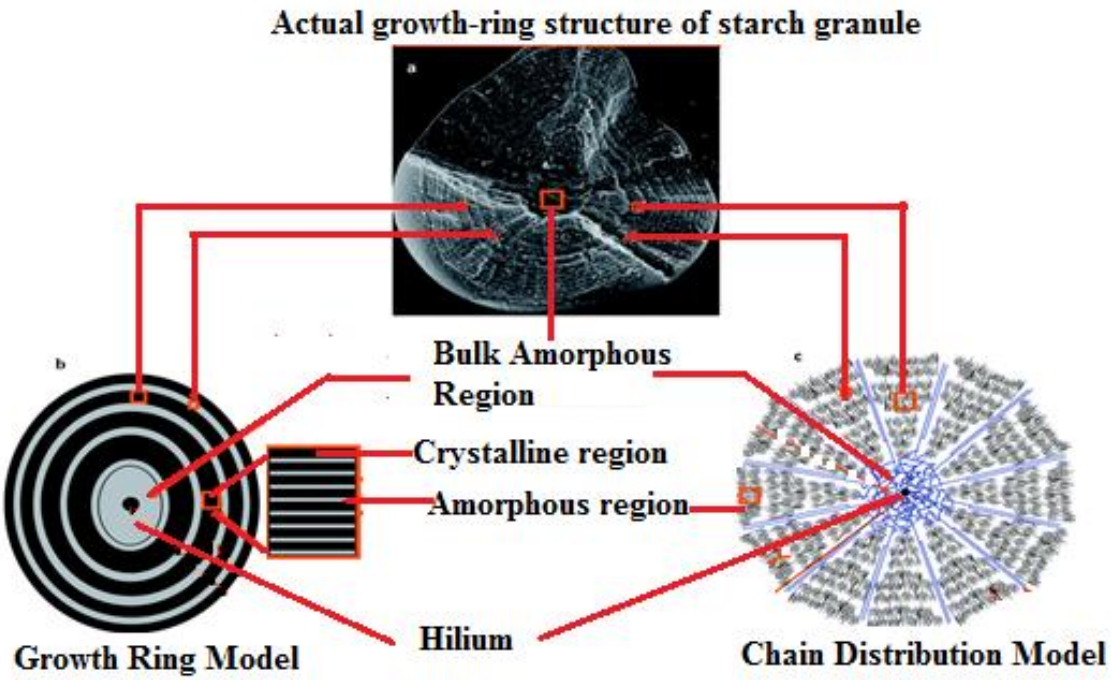

Figure 3. Growth ring model and chain distribution model to explain starch granule structure.[72] In general, there are areas of alternating amorphous and crystalline regions which self-assemble to form large granules. Reproduced with permission.

1.6 Crosslinking of Starch

Depending on the application, it may be necessary to increase resistance to shear stress for typical processing applications.[75] A hydroxyl group on starch could, through some basic chemistry, be linked to another hydroxyl group from another starch chain with a bifunctional small molecule. This results in the formation of a crosslink between the two chains. Crosslinking smaller starch particles provide more stability and resistance to degradation. Several molecules have been used to crosslink starch in the past, such as glyoxal[76], sodium trimetaphosphate (STMP),[77] sodium tripolyphosphate (STPP),[77] citric acid,[78] and epichlorohydrin.[75] While epichlorohydrin by itself has shown evidence of reproductive toxicity,[79] the crosslinking reaction

forms “glycerol bridges”, which are considered non-toxic. Citric acid could be used but the crosslinking method involves using harsh conditions, and is time consuming.[78]

1.6.1 STMP Crosslinking

STMP is a biocompatible and non-toxic crosslinker regularly used for starch. It consists of three phosphate groups arranged in a cyclic manner, with alternating phosphorus and oxygen atoms completing a 6-membered ring. It is a FDA-approved thickening agent and, like most cross-linkers for starch, it provides more mechanical stability to shear in food processing.[69] The overall reaction scheme for the crosslinking of starch by STMP is shown in Figure 4. At a sufficiently high alkalinity (pK_a for hydroxyl groups ~12.6[80]), the hydroxyl groups on the sugar rings become deprotonated (forming an alcoholate) and the oxygen ion can attack one of the phosphorus atoms on the ring through a nucleophilic reaction mechanism. Another hydroxyl group on starch would attack the same phosphorus atom, forming a phosphate bridge between the two sugar rings.

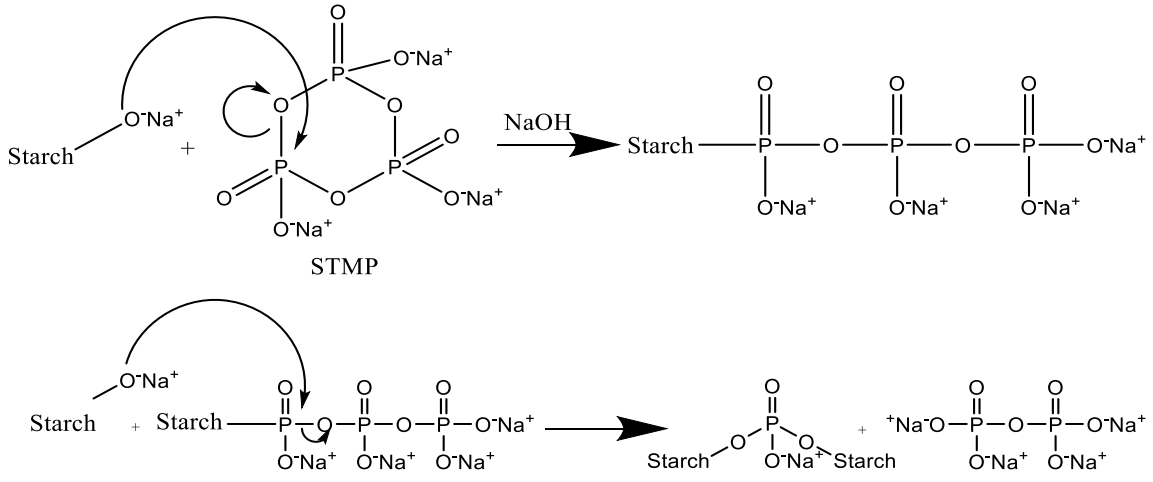

Figure 4. Overall reaction scheme for starch crosslinked by STMP. A phosphorus atom on the STMP ring will undergo nucleophilic attack by a starch alcholate group, forming a triphosphate.

Another starch alcholate will attack the same phosphorus atom, forming a distarch monophosphate.

In reality, the crosslinking reaction is much more complicated, and it is somewhat inefficient. Sang *et al*. performed extensive ^{31}P-nuclear magnetic resonance (NMR) studies to determine the extent to which side reactions may dominate the crosslinking reaction.[81] A summary of the proposed reactions is shown in Figure 5. The first step of the reaction is the nucleophilic attack of the starch alcholate on the STMP ring to form monostarch triphosphate. At this point, two different reactions may occur if the pH is maintained between 11.5 and 12.5. The first is with another starch alcholate attacking the same phosphorus forming the desired crosslink (distarch monophosphate). The second reaction that may occur is with a hydroxyl group (supplied by alkaline conditions) attacking the same phosphorus, forming monostarch monophosphate, which is quite stable. Lastly, a peeling reaction can occur at lower pH where a phosphate group from the monostarch triphosphate can migrate off, eventually (in the presence of water) forming the HPO_4^{2-} anion. These findings were also supported by Lack *et al*., who performed similar studies using a model system and arrived at a similar conclusion.[82]

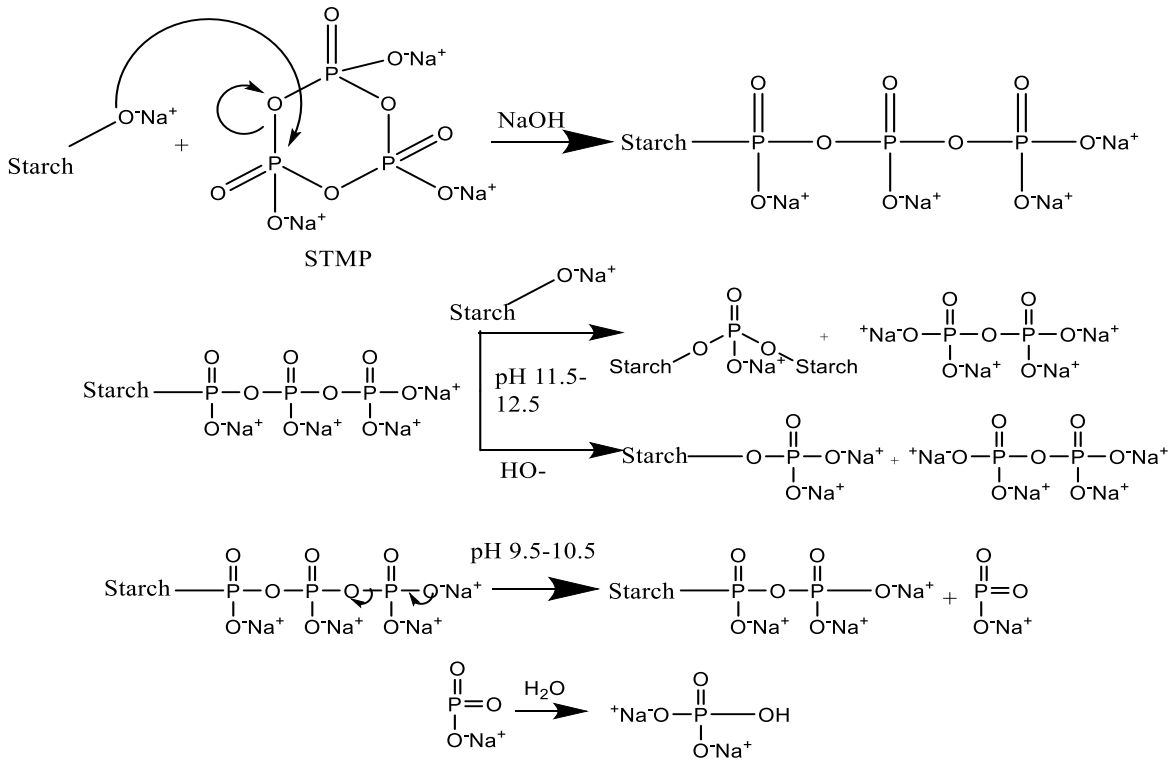

Figure 5. Detailed mechanism for starch crosslinking by STMP. Figure derived and redrawn from Sang *et al*.[81] Reproduced with permission.

Only 50% of the STMP added initially actually reacts with starch to form the triphosphate. Of that amount, ca. 20% goes on to form the distarch monophosphate (the other ca. 80% being various other phosphate species, including triphosphates and pyrophosphates).[82] Therefore, with respect to the amount of STMP that is added, the reaction itself is relatively inefficient. The addition of salts (such as sodium chloride) is known to increase the efficiency of the reaction,[83] most likely due to increased screening of the charges of the negatively charged phosphate groups, allowing for more nucleophilic attack.[77] The kinetics of the crosslinking is typically quite slow at room temperature and crosslinking of bulk starch may take days.[77] This crosslinking process is also temperature dependant, with higher temperatures being shown to result in more phosphorus incorporation.[84]

1.7 Starch Nanoparticles for Drug Delivery

Bulk starch would not be useful for applications like drug delivery since the size of the granules are simply too big. Therefore, a great deal of interest has been placed in making starch particles on the nanoscale. To that end, there are several processes which have already made strides in this field and which can be placed into three classes: hydrolysis, regeneration and mechanical treatment.[85]

Hydrolysis is a common reaction in which water is used to break a chemical bond.[86] In polysaccharides, such as starch, this reaction normally would take place at the position of the α (1->6) glycosidic bond in amylopectin and is normally performed using strong acids.[87,69] More recently, this method has been used to make crystalline starch nanoparticles.[85] Many studies have confirmed this behaviour and the size of the nanocrystals appeared to depend on the source of the starch, but generally was between 10-80 nm in size.[88,89] In these cases, the acid was able to dissolve the amorphous regions of starch, leaving crystalline nanodomains present. The crystallinity was confirmed by X-ray diffraction studies. Amylase, an enzyme which degrades starch, was also reported to form 500 nm nanocrystals through hydrolysis.[90]

Regenerative methods of producing starch nanoparticles (SNPs) include precipitation, reactive extrusion, and cocrystallization[85]. For example, Kim and Lim utilized the property of complex formation between amylose and polar lipids (in this case, butanol) and combined it with enzymatic hydrolysis to form starch nanocrystals of sizes between 28-51 nm with very low yield amounts (ca. 1%).[91] EcoSynthetix, a company based in Burlington, ON, have used a proprietary reactive extrusion technique to make starch-based biopolymer latex nanoparticles.[92]

Nanoprecipitation has also been used to make starch nanoparticles, as well as other polymeric nanoparticles.[93–95] With starch, crosslinking of the particles was performed using STMP or sodium tripolyphosphate (STPP). STPP is similar to STMP in that a phosphate linkage is formed between the two starch chains, but the mechanism is slightly different.[77] In some of these studies, the ultimate application was drug delivery, which provides an idea of the state of the field. For example, Nagger *et al*. synthesized STPP-crosslinked starch nanoparticles of sizes less than 60 nm using TWEEN 80 as a surfactant.[96] They encapsulated a non-steroidal anti-inflammatory drug (NSAID), diclofenac sodium (DS), and observed an optimal entrapment efficiency of 95%, with the release being modulated by the amount of crosslinking present. The ultimate application was transdermal drug delivery. Narayanan *et al*. used nanoprecipitation to synthesize STMP crosslinked hydroxyethyl-starch nanoparticles and loaded two NSAIDs, ibuprofen (IB) and indomethacin (ID), within the starch particles.[67] In this study, the precipitation was carried out in methanol (stabilized with lecithin) and crosslinking was performed for 3 hours at 47 ^{o}C in alkaline conditions. Particle sizes were ca. 150 nm in water and slightly higher in phosphate buffer saline (PBS). Little *in-vivo* toxicity was seen in rats and the encapsulation efficiency for IB and ID were ca. 75.41% and ca. 77.38% respectively.

Lastly, mechanical agitation has been utilized to form starch nanoparticles. This agitation could be provided by ultrasonication, high shear mixing, or high pressure homogenization/microfluidization.[85,97] Shi *et al*. used high pressure homogenization combined with an emulsion to produce STMP-crosslinked particles of sizes between 100-300 nm.[98] In this particular method, the emulsion droplets served as a reaction vessel for the crosslinking to occur and parameters that determined particle size were surfactant concentration, starch concentration, passes in homogenizer, pressure, as well as the ratio of dispersed phase/continuous phase. Xiao

et al. conjugated SNPs with folic acid (FA)-polyethylene glycol (PEG) using an emulsion-based method and crosslinked them using $POCl_3$.[99] Folic acid is able to be internalized more selectively by cancer cells as they have an overabundance of folic acid receptors. They were able to see a maximum doxorubicin drug loading of 25 μg/mg SNPs and observed higher internalization of the FA-PEG-SNPs inside cancer cells compared to normal cells. However, beyond this study, there have been very few reports of SNPs specifically for drug delivery into cancer cells.

1.8 Previous Work from the Liu Lab-ECO collaboration

In the past, Howard Tsai of the Liu lab investigated the efficacy of starch-based, experimental grade biopolymer latex nanoparticles (BLNPs) supplied by EcoSynthetix, for drug delivery. These particles, prior to any chemical modification had had a dominant particle size of ~20-150 nm and were easily dispersed in water.[92,100] It would be difficult to observe any uptake of the BLNPs into cancer cells, and so functional molecules such as dye or dye labelled DNA were conjugated on the surface of the particles. The uptake of the BLNPs in cancer cells was visualized using confocal microscopy.

1.8.1 Cellular Uptake

BLNPs were conjugated with both dye and dye-labelled DNA aptamers for visualization of the uptake in "Henrietta Lacks" (HeLa-a cervical cancer cell line) cells using confocal microscopy. The AS1411 aptamer was chosen as it has an affinity to nucleolin, a protein found overexpressed on many cancer lines (including HeLa). Confocal images of functionalized BLNPs in cells are shown in Figure 6. The nuclei of the cells are labelled with 4',6-diamidino-2-phenylindole (DAPI), which stains DNA inside the nucleus and is shown in the blue channel.

The cytoplasm of the cell is typically stained with a fluorescein labelled phalloidin, which binds strongly to actin inside cells and seen below in the yellow channel. In this case, the BLNPs were stained with a green fluorescein isothiocyanate (FITC) dye and the aptamer was labelled with a red dye (usually a rhodamine derivative). Internalization of dye-labelled BLNPs was seen, even without conjugated aptamer. This could be attributed to the EPR effect mentioned before, where smaller particles tend to accumulate in cancer cells as a means of passive targeting. Once aptamers were functionalized on the surface of the particle, no significant increase in the internalization was seen, even with higher amounts of aptamer. The dye fluorescence on the green channel was co-located with the red fluorescence on the red channel, confirming that the DNA aptamers and the dye were located on the particles.

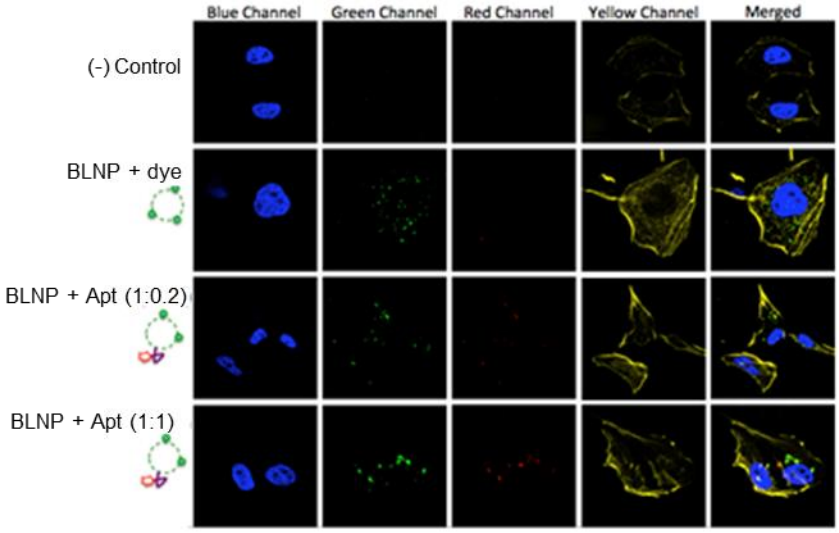

Figure 6. Confocal microscopy of loaded BLNPs in HeLa cells.[101] Experiments performed by Tsung-Hao Tsai. Reproduced with permission.

As a comparison, aptamer and dye-loaded liposomes were synthesized and compared to the BLNP uptake. Liposomes, as discussed before, are among the oldest known drug delivery vehicles and are well understood. The confocal images of the uptake are shown in Figure 7.

Conjugated liposomes appear to be internalized by the cells significantly more than the BLNPs, even at fairly high DNA concentrations for loading of the BLNPs.

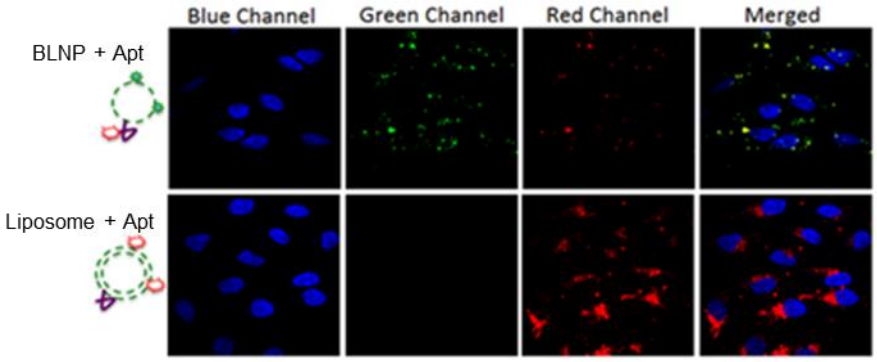

Figure 7. Comparison of BLNPs and liposome internalization.[101] Experiments performed by Tsung-Hao Tsai. Reproduced with permission.

1.8.2 Limitations of BLNPs for Drug Delivery

To attempt to explain why the BLNPs directly received from EcoSynthetix were not very suitable for cell internalization (and by extension, drug delivery), it is necessary to consider the size of the particle, as well as the nature of internalization itself. When aptamers bind to receptors on the cell surface, the process of internalization begins where cell membrane collapses to engulf the particle in a vesicle, pushing it into the cytoplasm. This internalization is known as receptor-mediated endocytosis. This phenomenon is promoted by the multi-valence effect, where the more aptamer on the surface of the particle, the stronger the binding will be and the more internalization will occur.

As mentioned before, the particle size of the BLNPs was between 20-50 nm. Liposomes may have variable size but in drug delivery, typical diameters are between 100-200 nm.[102] By virtue of surface area alone, there would be much higher coverage of DNA on each liposome compared to the BLNPs, as shown in Figure 8. One possible solution would be to use more DNA

aptamers to get more coverage on the surface of the BLNP. However, this is not very cost-effective. If the assumption is made that the BLNPs molecular weight (MW) is 1000000 g/mol (based on the molecular weight of amylopectin), and the MW of the DNA aptamer is known to be ca. 10000 g/mol (for a 30 nucleotide aptamer), then 8 aptamers on the surface of the particle would already be 8% of the MW of the BLNP (as an example). In a 100 nm liposome, the MW is ca. 76000000 g/mol. If we keep the same density for the BLNPs, from previous research, 200 aptamers would attach to the surface of the liposome[103]. Therefore, this corresponds to just 2.6 % of the molecular weight of the liposome. In a 1:1 molar ratio of BLNPs/liposome:DNA, for every gram of BLNP that is used, 10 mg of DNA aptamer is used, whereas for a liposome, ~131 µg is used. This corresponds to using ~76 times more DNA to get a similar loading in BLNP, compared to a liposome. DNA is significantly more expensive than starch, and therefore, by simple scaling, it would be 76 times more expensive to use BLNPs compared to liposomes.

Another aspect of the small particle size lies in the drug loading capacity. In the long run, drugs would be loaded into the porous starch structure. Previous drug loading studies with these nanoparticle showed that the loading capacity was only 0.054%. If each particle was assumed to be spherical, then a small sphere such as the BLNP would have a certain drug loading within it. Evidently, this drug loading is limited by the volume and thus would be a function of the radius of the sphere. If the radius of the sphere were to be increased by 10, then the volume would increase by 1000-fold (volume scales to the third power of radius). Subsequently, the drug loading would increase by 1000-fold as well. Ignoring the cost of the vehicle itself, the main factor to consider (economically) is how many drug molecules each aptamer may carry. In that regard, the drug/aptamer ratio becomes important. Aptamer coverage on the BLNP surface is

limited by surface area, while drug loading is limited by volume. Therefore, increasing the particle size by 10-fold would increase the drug/aptamer ratio by 10 fold by simple scaling.

The ideal SNP would be in the range of 80-300 nm, with a high molecular weight so that more drug molecules could be loaded into porous starch structure, and for more aptamer coverage to exploit the multi-valence effect in cellular uptake. It must still be small enough to be internalized into the cell in the first place, and should ideally be smaller than 300 nm. Nanoparticles that are too large are easily cleared by the body. Modification with STMP would also add a highly negative charge to the particle and potentially further improve the drug loading capacity.

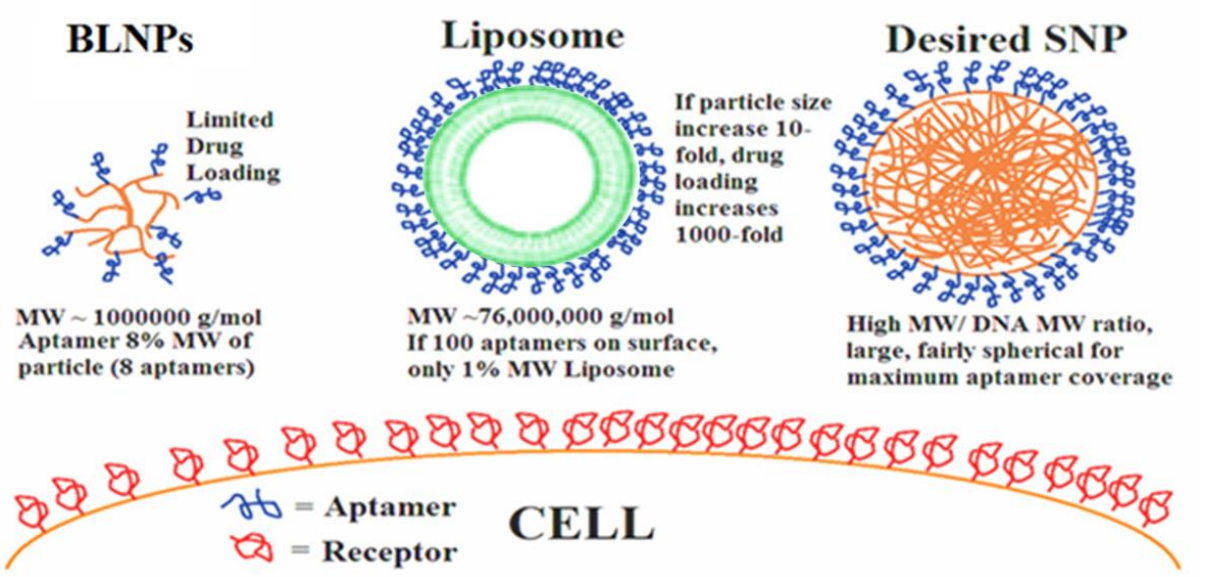

Figure 8. Limitations of non-crosslinked BLNPs for targeted drug delivery. Low surface coverage of DNA aptamer and potentially low drug loadings provide evidence for the need of a larger particle. Picture of liposome reproduced with permission.[104]

1.9 Research Goal and Implementation

With all the previous work in mind, the challenge lay in making larger starch nanoparticles for purposes of drug delivery as outlined in Figure 9. Free starch chains would be

crosslinked by STMP in a controlled manner to form high MW particles to satisfy the requirements from previous studies, followed by conjugation with DNA aptamer for cell-internalization studies. Ideally, these new nanoparticles would have a superior performance the BLNPs studied previously.

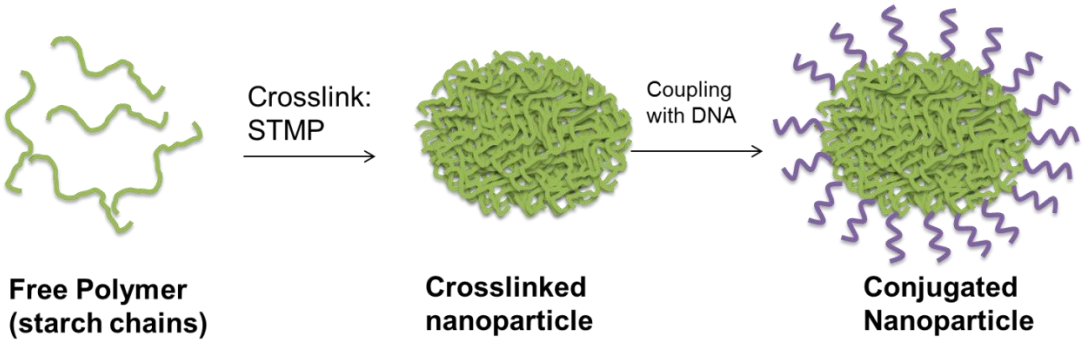

Figure 9. Confining crosslinking of starch chains to form nanoparticles followed by conjugation with DNA aptamer.

Chapter 2. Synthesis and Characterization of Phosphate Crosslinked Starch Nanoparticles

2.0 Introduction

To confine the particle size to sub-micron regimes, emulsions (more specifically, W/O emulsions) could be used, as discussed previously. Since the STMP is hydrophilic, it will partition into the water phase. The size of the particle is determined by the droplet size during the emulsion process as the particles would be internally crosslinked within it. Without access to powerful mixers (such as high pressure homogenizers and high-power ultrasonicators), W/O emulsion droplets are mostly confined to sizes greater than 1 μm.[105] Despite this, several low-energy approaches have been found to produce nanoemulsions (emulsion droplets with size between 20 and 500 nm). One of these approaches, phase inversion emulsions (PIEs), have attracted some interest in recent years due to its ease and scalability.[105–107]

Typically, if one were to homogenize a mixture of a water phase and an oil phase in the presence of a surfactant, an emulsion is formed where one phase (the dispersed phase) is suspended in the other phase (the continuous phase) as droplets. The resulting emulsion formed can be oil-in-water (O/W) or water-in-oil (W/O) depending on the type of surfactant used. For example, if a hydrophilic surfactant is used, an O/W emulsion can be made. The opposite is true for a hydrophobic surfactant. Hydrophilicity of a surfactant is determined by the hydrophile-lipophile balance (HLB), which has a value between 0 (extremely hydrophobic) to 20 (extremely hydrophilic).[108] A general rule of thumb is that a surfactant with HLB > 10 will typically stabilize an O/W emulsion at room temperature and one with HLB < 10 will stabilize a W/O emulsion.

As mentioned previously, a hydrophilic surfactant could be used to prepare an O/W emulsion. However, non-ionic surfactants which are hydrophilic at room temperature may not retain this behaviour at higher temperature. In fact, many of these surfactants become significantly more hydrophobic with increasing temperature. This is due to the dehydration of the polar hydroxyl head groups, effectively weakening the interaction of the surfactant with water.[109,110] The HLB decreases and the surfactants become more lipophilic. Therefore, heating an aqueous solution containing a hydrophilic surfactant would eventually cause the solution to turn cloudy and phase separate from the water. This is called the cloud point of a surfactant and is influenced by a variety of factors. Increasing salinity or adding alcohol causes the cloud point to change as it further interferes with the polar interactions of the water molecules and the head group of the surfactant. [111]

In an O/W emulsion stabilized by these non-ionic surfactants, the O/W emulsion becomes a W/O emulsion at higher temperature in a process known as phase inversion as shown in Figure 10. The temperature at which the phase inverts is known as the phase inversion temperature (PIT). At T<PIT, the O/W droplets are stabilized in solution by the surfactant. Once T=PIT, the surfactant becomes sufficiently hydrophobic that it does not necessarily stabilize one phase *vs* the other and the result is a bi-continuous phase within the initial oil droplet. At T>PIT, the surfactant becomes even more hydrophobic and would stabilize a W/O emulsion more readily. The droplet size of the resulting W/O emulsion is typically much less than the initial O/W emulsion because the phase inversion is constrained within each individual droplet. In fact, nanoemulsions (emulsions with droplet size <100 nm) have been reported using this phase inversion principle by lowering the temperature after an initial phase inversion.[112] However, these nanoemulsions were O/W, and therefore not useful for the STMP-SNP synthesis.

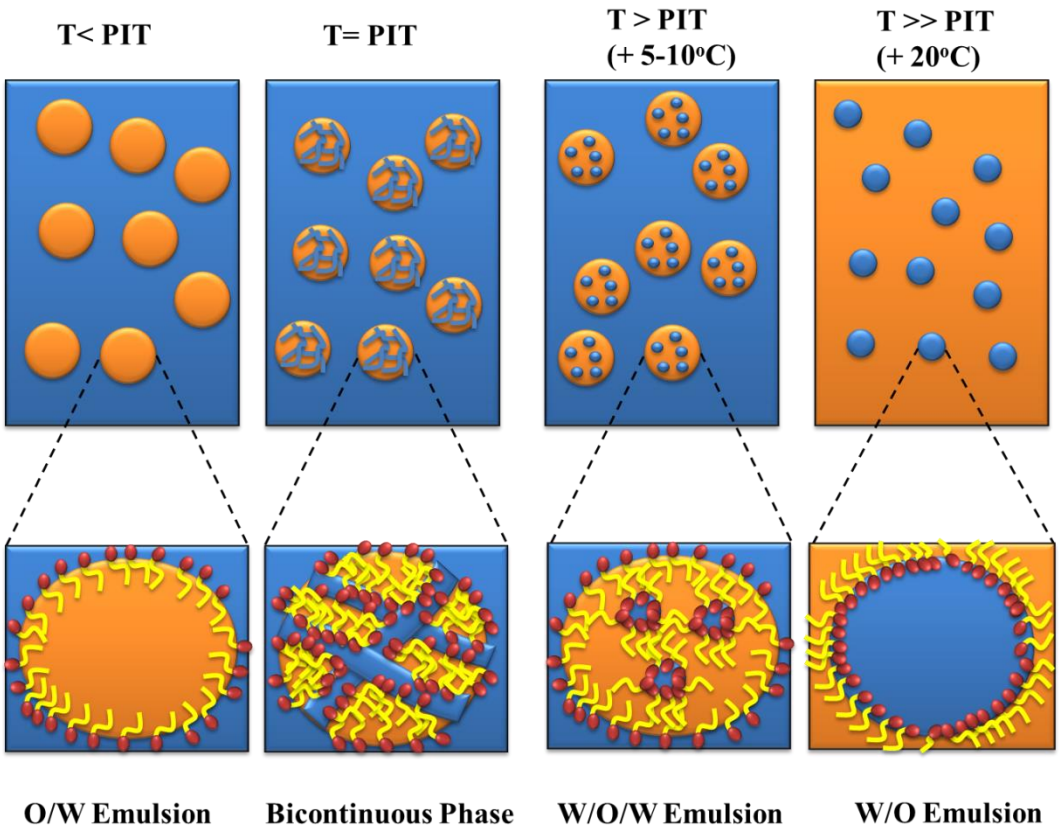

Figure 10. Concept of phase inversion emulsion. Certain anionic surfactants become more hydrophobic with temperature resulting in an inversion of a W/O emulsion to an O/W emulsion.

For SNP synthesis using phase inversion, the basic concept is shown in Figure 11. In brief, an oil phase is homogenized with a water phase containing fully cooked starch. Once the O/W emulsion forms, the temperature is raised to a temperature greater than the PIT for the particular surfactant and reaction conditions used. Once the phase inversion has completed, STMP would be added and the reaction would be allowed to proceed for 1 hour, forming internally crosslinked nanoparticles. EcoSynthetix, the collaborating company for this project, owns a patent where they describe the exact protocol for the formation of starch nanoparticles using this process.[107,113] Paraffin oil was used as the oil phase, with Tween 85 used as the surfactant. Tween 85 is an anionic surfactant with a critical micelle concentration (CMC) of 0.09 mM and a HLB of 11.[114,115] As such, it is already relatively hydrophobic (compared to other

hydrophilic stabilizers) but will initially form an O/W emulsion at low temperatures. To decrease the phase inversion temperature further, 0.3 M NaCl was used. Apart from this function, NaCl is a known catalyst of the STMP crosslinking reaction as it screens electrostatic repulsion of the phosphates for nucleophilic attack.[107] As reported by the patent, the phase inversion temperature of this emulsion is 25°C. Slight modifications were made to this procedure to optimize the amount of STMP needed to induce nanoparticle formation, leaving the parameters responsible for phase inversion (Tween 85 concentration, NaCl concentration, and volume fractions of oil and water phase) constant.

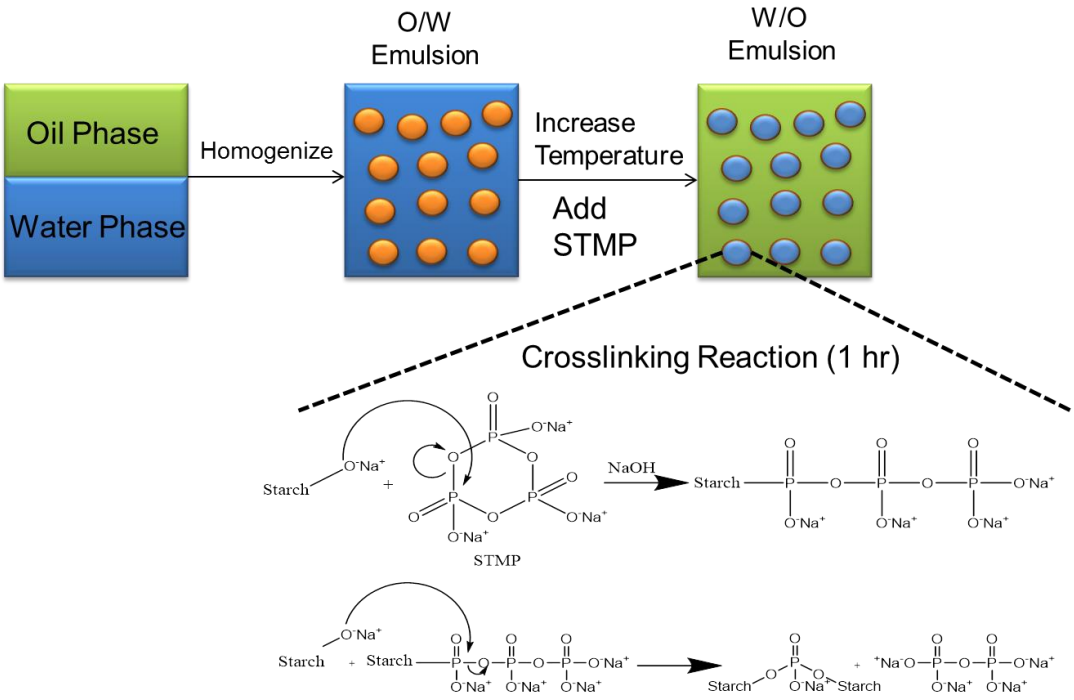

Figure 11. Schematic for STMP-SNP synthesis using PIE. Initially, an O/W emulsion is formed which, after an increase in temperature, becomes an O/W emulsion. The STMP is added so that the crosslinking reaction occurs within the emulsion droplet.

2.1 Materials and Methods

Cooking of Starch Granules. Typically, 46.8 g of waxy maize starch was dispersed in 1 L of deionized water. To this mixture, 20.8 g of NaCl and 11.7 g of NaOH was added, and the whole was brought to 55^{o}C for 2 hours. The solution was allowed to cool and stored at 4^{o}C until ready for use.

PIE for STMP-SNP Synthesis. In a typical reaction, 35 g of Tween 85 was dispersed in 600 mL of paraffin oil (oil phase) using a Silverson L4H high shear mixer stirring at 3000 RPM. Once the surfactant was fully dispersed, 400 mL of the cooked starch/NaCl solution in NaOH (water phase) was added and the shear rate was increased to 7500 RPM to form the emulsion. The temperature after complete homogenization of water and oil phase was ~18^{o}C. The shear force acting on the emulsion was enough to increase the temperature significantly, without any external heating required. At 55^{o}C, STMP was added in solid form at various concentrations to initiate the crosslinking reaction. The amount of STMP added was varied with respect to the amount of starch in the reaction. More specifically, it was expressed as a mole percentage of the anhydroglucose units (AGU) of starch used in the reaction. Taking 5 mol % STMP as an example, there would be 5 STMP molecules for every 100 AGU in starch. To calculate the mass of STMP to be added the following formula was used

$$m_{STMP} = X * \frac{n_{AGU}}{100(1-X)} * 305.885 \frac{g}{mol}$$

Where m_{STMP} was the mass of STMP to be added, X was the desired mol % STMP, n_{AGU} was the number of moles of AGU (MW_{AGU}=162 g/mol) used and 305.885 g/mol is the molecular weight of STMP. Samples were synthesized using different values of X: 0, 1, 5, 10, 30 and 50

mol% STMP. The STMP would partition in the water phase as it was completely insoluble in the oil phase. The reaction was then allowed to proceed for 1 hour at 70^{o}C.

To stop the reaction, 3 g of 37% HCl was diluted in 200 mL water and added to the emulsion. This neutralized the basic water phase so that nucleophilic attack of the starch hydroxyl groups to the STMP would be minimized and the crosslinking reaction stopped. The temperature was then brought down to 20^{o}C so that the continuous phase is aqueous (reversion to O/W emulsion). The particles were then precipitated using ethanol. To remove surfactant, the precipitate was washed three times with absolute ethanol and filtered using Buchner filtration. The nanoparticles were then dispersed in water and placed in a separatory funnel and allowed to stand so that oil could partition to the top of the dispersion. The water phase was then collected and any remaining oil was set aside for recycling. This was repeated 3 times to ensure any oil was removed. Finally, the sample was placed inside 10 kDa MW cut-off membrane for dialysis in a 1:10 ratio to dialysate to remove phosphate and chloride salts. Initially, the sample was dialyzed against 10 mM NaCl dialysate to lower the concentration gradient of salt from inside the membrane. This would prevent too much water from entering the membrane and rupturing it. It was then lowered by increments of half until day 4, when no salt was added. Dialysis was continued for 6 days, with initial dialysate changes occurring every 3 hours. After day 3, the dialysate was changed twice per day. Once dialysis was complete, the sample was frozen and stored at -20^{o}C for lyophilisation.

Dynamic Light Scattering and ζ-Potential. In a typical measurement, 1 mg STMP-SNPs were dispersed in 1 mL milli-Q water (final concentration: 1 mg/mL) and placed in a low-volume disposable sizing cuvette for measurement in a Malvern Zetasizer (Nano series). For ζ-

Potential, 1 mg of STMP-SNPs were dispersed in 1 mL 50 mM HEPES buffer (pH 7.6) and placed in a disposable zeta-cell for measurement. All measurements were performed at 25^{o}C.

TEM. The sample was prepared by dispersing 1 mg STMP in 1 mL water (final concentration= 1 mg/mL) before placing 15 μL on a holey carbon grid and allowed to dry overnight. The next day, the samples were imaged using a Phillips CM-10 electron microscope.

ESEM. A small amount of freeze-dried powder from the 0 mol% and 10 mol% samples were placed on an SEM sample holder with carbon tape. Compressed air was blown on the sample to remove loosely bound powder so that optimal imaging could be performed. The imaging was performed on a FEI Quanta Feg 250 ESEM.

^{31}P NMR. STMPs were dispersed in 1 mL milli-Q water at a concentration of 15 mg/mL and transferred to an NMR-tube. The proton-decoupled measurement was performed in an Avance 500 NMR spectrometer operating at 500 MHz (^{1}H) and 202 MHz (^{31}P) using phosphoric acid as a reference and without a solvent lock. All samples were run with a delay of 5 seconds, a pulse width of 2.8 seconds and a sweep width of 398.35 ppm.

Water Retention Studies. STMP-SNP samples prepared with different mol % STMP were dispersed in 1 mL water at a concentration of 15 mg/mL in a micro-centrifuge tube. These tubes were pre-weighed before the solution was placed in the tube. The samples were then centrifuged at 15000 RPM for 20 minutes. After centrifugation, supernatant was removed and the tube was re-weighed with the swollen product. The mass of the tube recorded before the experiment, as well as the mass of SNP present (15 mg) was subtracted from the final recorded weight to find the amount of water retained. For studies with salt, the sample which yielded the highest water retention (30 mol% STMP) was dispersed at a concentration of 15 mg/mL in 1 mL

water in various pre-weighed tubes. Two salts (NaCl and $MgCl_2$) were then added at increasing concentrations. The samples were then centrifuged, the supernatant decanted, and weighed.

2.2 Results and Discussion

During the synthesis, several characterization techniques were performed to ensure that the intended processes were occurring. These included polarized light microscopy to ensure cooking of starch, optical microscopy to determine droplet size and conductivity measurements to determine the phase inversion temperature of the emulsion. In addition, several characterization methods were employed to determine the physical and chemical properties of the prepared STMP-SNPs. These include: dynamic light scattering (DLS), transmission electron microscopy (TEM), scanning electron microscopy (SEM), ^{31}P nuclear magnetic resonance (NMR) spectroscopy, ζ-potential, and water retention studies.

2.2.1 Synthesis of STMP-SNPs

First, complete cooking of starch needed to be confirmed before the PIE procedure could be initiated. If there were any bulk starch granules left in the water phase, crosslinking would occur from the granule, resulting in a significant increase in particle size. The complete dissolution of starch was confirmed by light microscopy in Figure 12 with (A) and without (B) polarizers. If crystalline domains (such as those found in starch granules) were present, they would interact with polarized light giving rise to contrast from the background. No evidence of starch granules were seen after 2 hours of cooking as there appeared to be no granules left to interact with the polarized light.

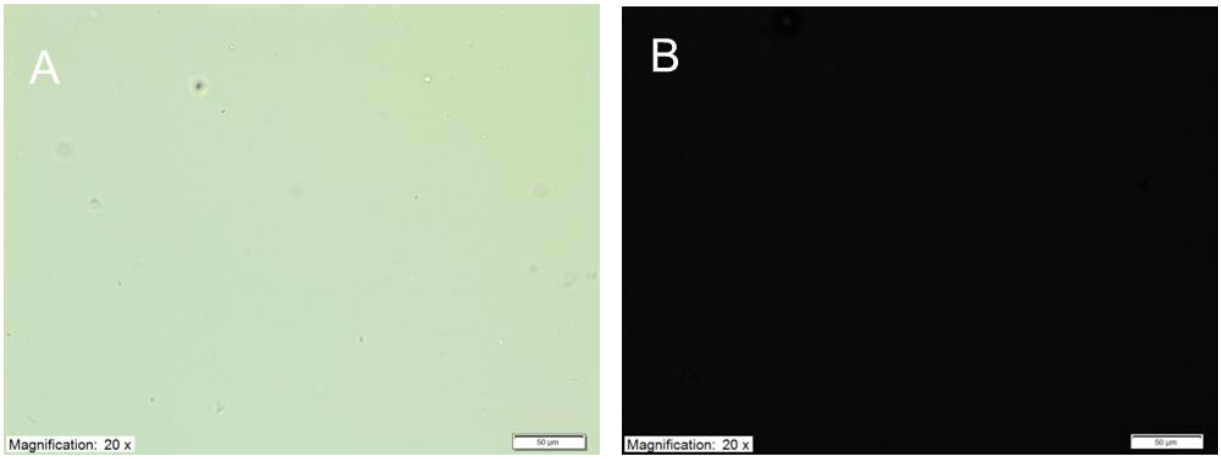

Figure 12. Light microscopy of cooked starch with (A) and without (B) crossed polarizers.[113] Since there was no signal present with the polarizers, no crystalline granule regions were present; the starch was fully cooked.

As mentioned previously, Tween 85 was the stabilizer used for this emulsion and its chemical structure is shown in Figure 13. The four polar polyethylene glycol heads serve as the hydrophilic stabilizer, while the three fatty acid tails serve as the hydrophobic stabilizer. Compared to many other Tween-based surfactants, it is quite hydrophobic and would just barely stabilize an O/W emulsion at room temperature.

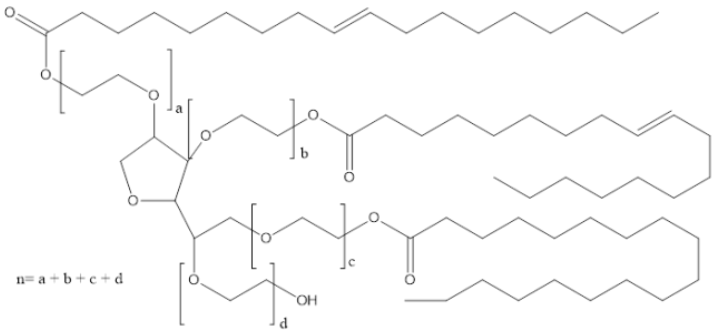

Figure 13. Chemical structure of Tween 85.

2.2.2 Characterization of Phase inversion

To characterize the emulsion process, two methods were employed: conductivity and light microscopy. The former was to confirm phase inversion from O/W to W/O and the latter was to determine the droplet size. Before phase inversion, water would be the continuous phase and as such, any conductivity measurement would yield a high value. This is especially true since there were NaCl and NaOH present, which facilitates current flow. On the other hand, after phase inversion, oil would be the continuous phase. Since there were no ions present in the oil phase, the conductivity would drop significantly upon phase inversion. Using this principle, the conductivity was measured as a function of temperature, as shown Figure 14. Before ~30^{o}C, the conductivity was high (~11 mS/cm) as water was the continuous phase. Beyond this temperature, there was a rapid drop in conductivity to ~100 μS/cm, correlating to the phase inversion of the emulsion. In addition, consistency of the emulsion changed significantly after phase inversion; below the PIT, the emulsion appeared thick and viscous whereas beyond the PIT, it appeared much thinner.

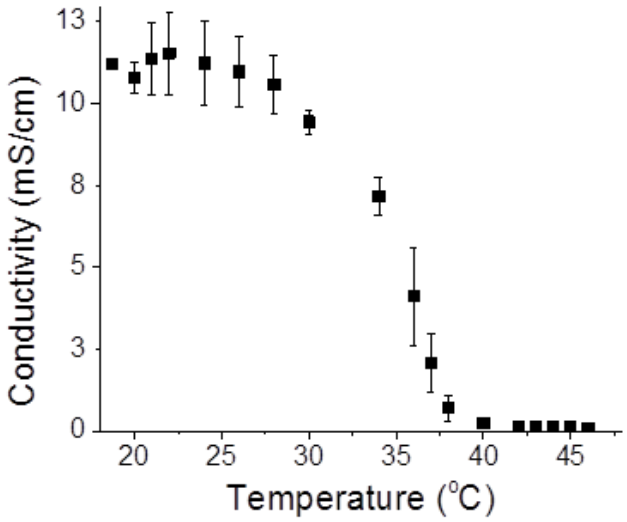

Figure 14. Conductivity measurements during phase inversion. A clear drop in conductivity is seen starting at 30°C, indicating the phase inversion process had begun. Once it levelled off, the process was complete.

The droplet size was characterized before (A) and after (B) phase inversion using optical microscopy as shown in Figure 15. Before phase inversion, droplet sizes were between 2-8 μm. After phase inversion, it was impossible to determine the droplet size as they were beyond the limits of the optical microscope resolution.

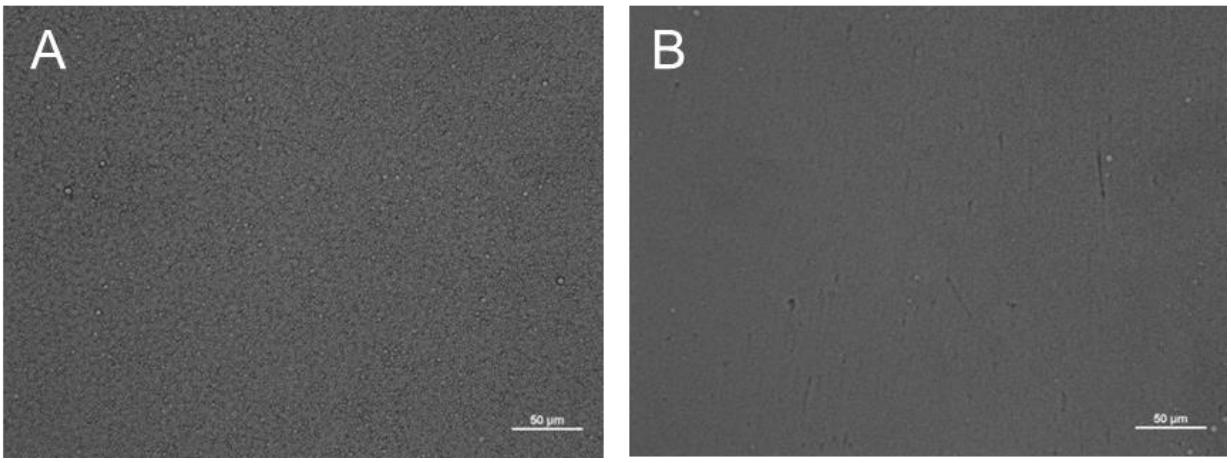

Figure 15. Optical microscopy of emulsion droplets before (A) and after (B) phase inversion. There was a very apparent decrease in droplet size after phase inversion, which could not be resolved from optical microscopy.

2.2.3 DLS and ζ-Potential

Dynamic light scattering (DLS) is used to measure the size of particles in solution.[116] In principle, a sample is illuminated by a laser light and the amount of scattering is detected. For a very small time period after an initial measurement, the amount of scattering will be the exact same as the time period before it. It could therefore be said that at that time period, there is a full correlation between the two measurements. However, as time increases, this correlation will decrease due to the movement of particles by Brownian motion. Assuming full correlation corresponds to "1" and no correlation corresponds to "0", a correlation function could be generated, which is normally in the form of an exponential decay.[117] Smaller particles move very quickly, and therefore the correlation function would decay to zero at a short time period after measurement begins. Larger particles move much more slowly and therefore the correlation at higher time periods would decay to zero at longer times after the beginning of the measurement. In an ideal case, the correlation function can be modeled by an exponential function, where a relaxation time could be obtained for a particular species in solution. This relaxation time is related to the diffusion coefficient of the particulate species in solution. Using the Stokes-Einstein equation, and known parameters like temperature and viscosity, the hydrodynamic radius could be obtained. This is done automatically by the instrument software and what is obtained is an intensity plot is generated from the correlation function which provides an idea of the population of particle sizes in solution.

In addition to DLS, ζ-potential measurements were also performed on the STMP-SNPs prepared. If a charged particle is in solution, then it will attract counter ions to its surface *via* coulombic interactions. This layer of counter ions is called the Stern layer. The concentration of

these counter ions decays with distance away from the particle and, this region is known as the diffuse layer.[118] Collectively, the Stern layer and the diffuse region are part of the electrical double layer. At a certain point, there is no excess of one ion over the other, which corresponds to the bulk liquid phase. However, some of these solvated counter ions move with the particle itself and are considered to be "attached" to the particle. The point in the electrical double layer where this "attachment" stops is known as the slipping plane. In principle, the ζ-potential measures the difference in electric potential between bulk liquid and the slipping plane. From this, information about the particle surface charge can be obtained.[118]

The intensity distribution of hydrodynamic diameter measured from DLS for samples prepared using different amounts of STMP is shown in Figure 16 A. Without STMP, the free starch chains appeared to have a hydrodynamic diameter between 30-40 nm. Normally, a high MW polymer such as starch would have a larger hydrodynamic radius in solution. However, exposure to shear forces used in the process would have likely reduced the size of the native starch chains (resulting in a lower hydrodynamic radius). When STMP was used, this diameter increased to between 300-400 at 30 and 50 mol%. In between these two extremes, there appeared to be a progression in the particle size from smaller to larger. This is unlike typical crosslinked nanoparticles, where there is a general decrease in particle size with crosslinker content. This increase was therefore likely due to the crosslinking of the starch chains within the emulsion droplets, resulting in a particle limited by the size of the droplets. Based on the sizes obtained at high STMP concentrations, it appeared that these droplets (and as such, the particles sizes) were between 200-400 nm. At lower concentrations, it was possible that less crosslinking was occurring and this limited the particle size to less than the droplet size. Apart from crosslinking, the mixture is being subject to very high shear forces which could also affect the particle size.

Such forces, in such conditions of pH and temperature, could be enough break the starch chains to smaller lengths, resulting in lower hydrodynamic radii (especially evident at lower STMP content).

The ζ-Potential measurements for each sample in pH 7.6 50 mM HEPES buffer is shown in Figure 16 B. There was a general increase in the negative surface charge of the particles with STMP concentration. Even at 1 mol % STMP, there was a great deal of negative charge imparted on the particles. Quite likely, there was some phosphorylation at lower STMP concentrations but the nature of these species was dominated by phosphates that were not necessarily the phosphodiester linkage between separate starch chains (such as monophosphates).

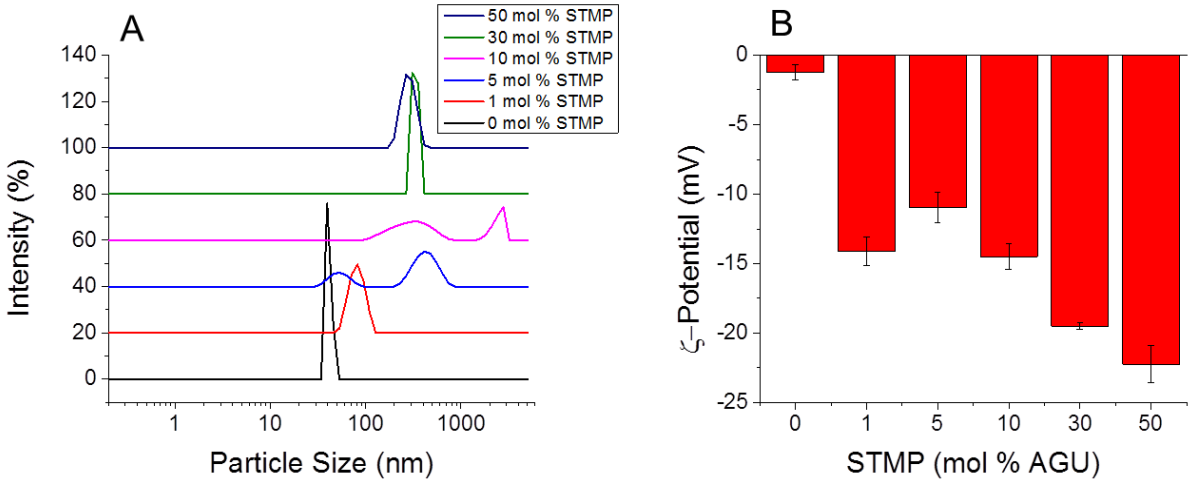

Figure 16. Dynamic light scattering (A) and ζ-Potential (B) measurements for the various synthetic formulations of STMP-SNPs. There is a clear increase in particle size and negative surface charge with increasing STMP content in the synthesis.

2.2.4 Transmission Electron Microscopy (TEM)

TEM is a widely-used technique to visualize nanoparticles. Samples are loaded at low concentration (so that there is a very thin layer of material) on to a conductive grid and placed into a vacuum chamber.[119] Electrons are fired at the sample at very high energy (100-1000 kV), either from a thermionic (where heat is used to release electrons) or a field effect emission (using a strong electric field). Electrons which interact with the sample are scattered, while others are transmitted through to a detector and an image is generated. TEM works best with electron-dense samples, such as metal nanoparticles, as the scattering would be much more obvious and detectable. With polymeric samples, such as starch, it is more complicated. Polymer chains themselves would not be able to be visualized since electrons may pass straight through them, without any reasonable contrast to the background. In addition, the high energy electrons would damage the polymeric sample quite easily. This being said, there are reports of crosslinked starch nanoparticles being imaged by TEM, likely due to the increase in electron density.[96,98]

TEM was performed on the STMP-SNPs at various concentrations of STMP and typical images are shown in Figure 17 A-F. Without STMP, small spherical particles of ca. 20 nm were seen. These may be due to dried appearance of the free starch chains, small droplets of oil remaining from the purification process, or simply an artifact of drying itself. At 1 mol % STMP, faint areas of darker, fibrous features indicated that there was indeed an effect on the particle morphology even with a small amount of STMP. Clear particles were seen beyond 5 mol% STMP where darker areas correspond to the dense, internally-crosslinked core of the nanoparticle, with lighter representing sparser crosslinking on the outer regions. These particles were not strictly uniform in shape but were confined between 100-700 nm in size, with isolated

larger (> 1 μm) and smaller (<100 nm) particles. In addition, individual chains in the crosslinked polymer network could be seen at higher concentrations of STMP. Based on this, it was more accurate to refer to this material as a nanogel as opposed to a solid particle. Since these nanogels were dried out for the TEM experiment, it may not necessarily reflect the solution morphology. This being said, the previously-obtained DLS data supports the TEM imaging, suggesting that the solution behaviour was not far from the dried morphology.

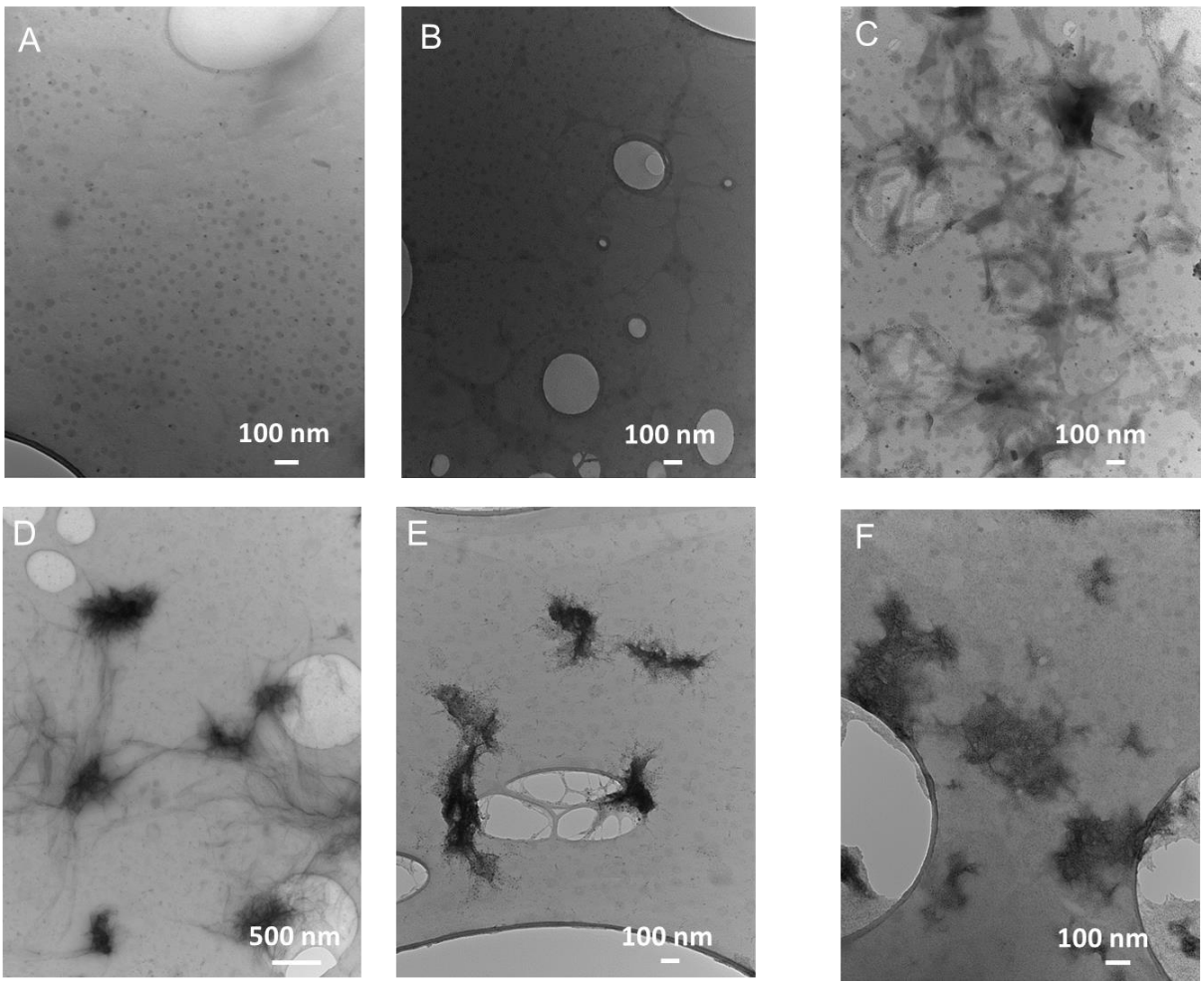

Figure 17. TEM Images of STMP-SNPs prepared using 0 (A), 1 (B), 5(C), 10 (D), 30 (E) and 50 (F) mol % STMP.

2.2.5 Environmental Scanning Electron Microscopy (ESEM)

SEM is another imaging technique that uses electrons to visualize samples at a much higher resolution than light. Unlike TEM, however, SEM relies on electrons that are scattered out of the sample upon bombardment rather than the electrons that are transmitted through the grid for contrast. The basic principle is that some electrons on the sample surface are ejected from the sample upon impact with the primary electron. These electrons (called secondary electrons) are then collected by an electric field where they hit a phosphor screen, emitting flashes of light. This light is then amplified using a photomultiplier tube and ultimately detected using digital electronics. The resulting 2-D image is a collection of intensities corresponding to the angle of incidence of the electrons on the surface of the sample.[120] High incidence angles result in more electrons being emitted, causing steeper morphologies to appear brighter. Typically, this is done on conducting samples such as metals since the electrons can flow through the material freely without building up at the surface. If non-conducting samples (such as SNPs), significant charge build-up at the surface causes charging effects that significantly lowers the quality of the image obtained.

A variation of this technique is environmental SEM (or ESEM), where chamber pressures are kept relatively high and water molecules are abundant in the sample chamber. As a result, charging artifacts are removed even in non-conducting samples and the image quality is improved.[120] Sample preparation for ESEM is unchanged from conventional SEM. ESEM was performed on the 0 mol % (A) and the 10 mol % (B) STMP-SNP samples as shown in Figure 18. Without STMP, no obvious morphologies or particle formation was observed. However, with 10 mol% STMP, spherical particles between 100-500 nm were observed (red arrows), consistent with both DLS and TEM obtained previously. It was important to note that the sample was

lyophilized prior to imaging with ESEM, unlike TEM where the sample was dried in air on the grid. This meant that the morphology obtained from ESEM would more closely reflect that in solution, and there would be no drying effects. Taken together with DLS and TEM results, the ESEM image for the 10 mol% sample suggests a uniformly spherical particle in solution. The size of the particle (between 100-500 nm in diameter) likely reflects the size of the emulsion droplets during the PIE emulsion process.

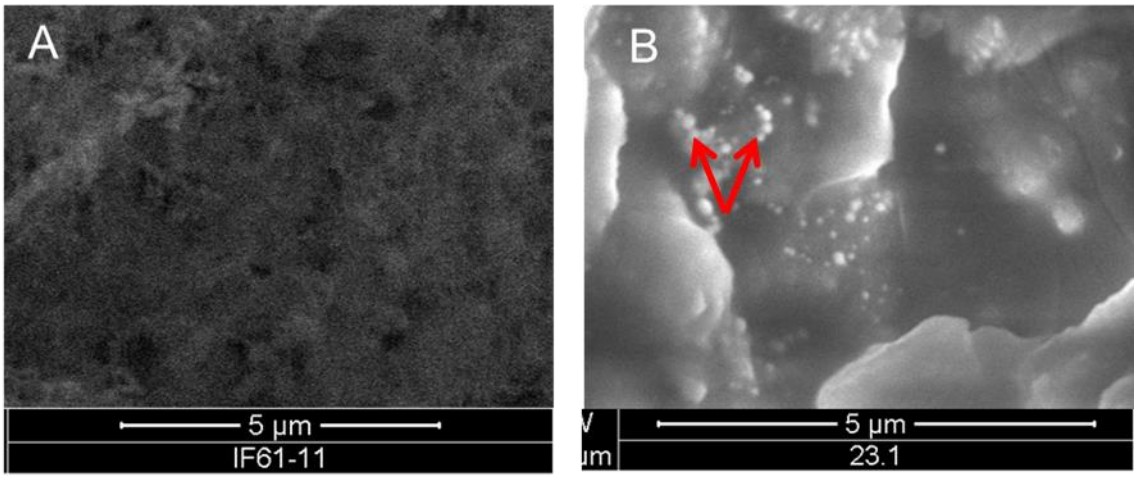

Figure 18. SEM images of samples prepared without STMP (A) and with 10 mol % STMP (B)

2.2.6 ^{31}P-NMR Spectroscopy

To gain an idea of the nature of the phosphate species present in the samples prepared, ^{31}P NMR spectroscopy was performed. Certain atomic nuclei, when placed in a magnetic field, can absorb specific wavelengths of light in the electromagnetic spectrum. This is due to the fact that these nuclei have special spin states which will either align with or against an external magnetic field.[121] For example, with a spin ½ nuclei, two spin states are present; one will align with the magnetic field and the other will oppose it. This generates an energy gap, the size of which is dependent on the specific nuclei present, and its local electronic environment. The spin

state of lower energy could be excited to a state of higher energy if electromagnetic radiation of a frequency corresponding to the characteristic energy gap was applied. This absorption of radiation by specific spin states in the external magnetic field forms the basis of NMR spectroscopy. As mentioned previously, the local electronic environment plays a major role in this energy gap. This is because electrons can also align themselves in the magnetic field to generate their own, weaker, magnetic field which opposes the external, stronger, magnetic field. Effectively, this shields the nuclei being probed from the external magnetic field, resulting in a different absorption radiation frequency. These changes are quite small, with shifts on the order of Hz over a MHz reference signal.[121] As a result, the ratio of the change to the reference is on the order of a 10^{-6}. Therefore, these values are typically multiplied by 10^{6} before analysis. This modified ratio is known as the chemical shift (δ) and is normally in the units of parts-per-million (ppm). The chemical shift can also be a negative number, as it is measured as a change relative to a reference frequency.[122]

Phosphorus (^{31}P), unlike many other nuclei studied using this technique, has a spin ½ nuclei of 100% abundance, meaning that all phosphorus atoms could be probed using this technique. This being said, ^{31}P-NMR, in general, is not quantitative; uneven nuclear-Overhauser effect (NOE) enhancement prevents any integration of the peaks.[123] However, the chemical shifts can provide evidence of crosslinking within the STMP-SNPs, and the other types of phosphate species present. In addition, the sharpness of the peaks would indicate whether there is covalent attachment to the polymer chain (broadened peaks) or whether inorganic phosphate species are simply embedded in the crosslinked nanogel non-covalently (sharper peaks). This reaction has been studied with starch, as mentioned previously.[81,82] The data obtained from NMR was

compared to literature reports consistent with the chemical shifts observed for assignment of the peaks.

The ^{31}P-NMR spectra for all samples prepared are shown in Figure 19 A-F. As expected, no organic/inorganic phosphorus species were detected for the sample prepared without STMP (Figure 19 A). At 1 mol % STMP (Figure 19 B), very small and poorly resolved peaks appeared at 0.56 and 3.53 ppm, potentially consistent with phosphodiester and monophosphate respectively. There was also the appearance of the outer phosphorus atoms of the starch triphosphate at -7.65 ppm. Based on literature, there should be a corresponding peak for the inner phosphorus of the triphosphate at ca. -20 ppm. However, due to the poor resolution obtained for this sample, this was not assigned. At 5 mol % STMP (Figure 19 C), multiple new peaks appeared indicative of more extensive phosphorylation. Between 0 and 5 ppm, there were 3 peaks. Based on the particle formation from TEM imaging, some crosslinking had occurred (as there would be no covalent phosphodiester linkages to hold the particle together). However, it was not clear which of these peaks corresponded to the phosphodiester or monophosphate. In addition, the sharp peak at 1.33 ppm seemed to indicate an inorganic species, potentially inorganic monophosphate that was not removed by dialysis. In addition, 3 peaks were seen between -5 and -10 ppm. One of the peaks may correspond to the α and γ phosphorus atoms of the triphosphate, another may be the same but for inorganic triphosphate and the last one may be for the presence of the diphosphate. Finally, the last peak at -21.8 ppm was likely to be the β phosphorus of the either the organic or inorganic triphosphate. For 10 mol % STMP (Figure 19 D), there were fewer peaks, and those that were present were quite broad. This was strongly indicative of only organophosphate species being present as opposed to inorganic phosphates. Likely, dialysis was very successful on this sample and as such, a cleaner spectrum was obtained.

This being said, the two peaks between 0 and 5 ppm were likely to be starch monophosphate or phosphodiester linkages, but it was not possible to distinguish between them. For 30 mol % and 50 mol % (Figure 19 E and F, respectively), there was even more significant broadening of the peaks between 0 and 5 ppm, likely indicating significant crosslinking of starch. In addition, several other peaks were seen, including the outer phosphorus atoms of the organic triphosphates and diphosphates between -5 and -10 ppm, with sharper peaks in this region corresponding to the inorganic analogues to these species. At these high concentrations of STMP, it was quite likely that even 6 days of dialysis was not enough to remove the high amount of inorganic by-products. Another complication could be that the crosslinking was so extensive, that it trapped unreacted and inorganic species within the crosslinked nanogel, preventing escape through dialysis processes.

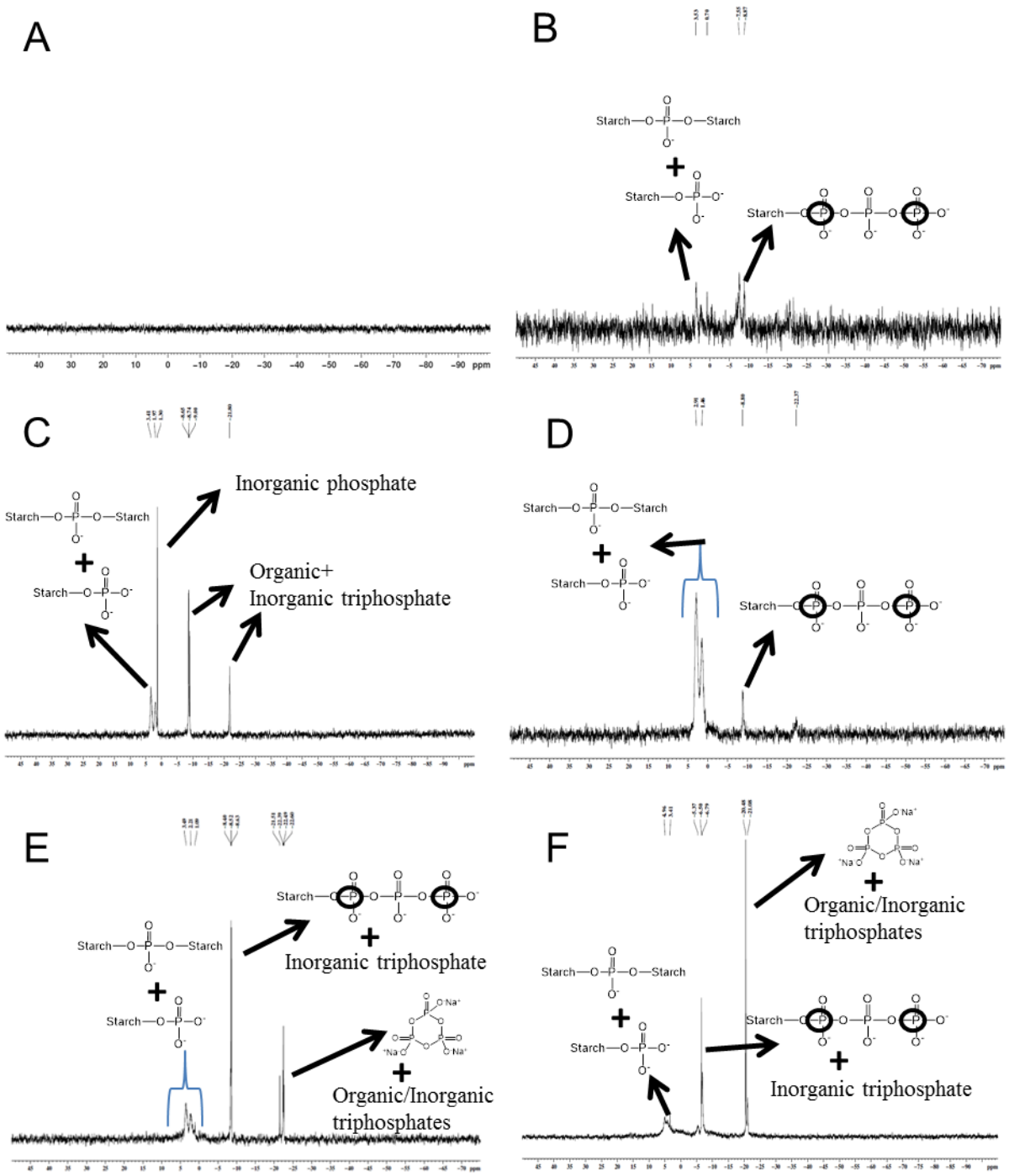

Figure 19. ^{31}P-NMR of samples prepared with 0 (A), 1 (B), 5 (C), 10 (D), 30 (E) and 50 (F) mol% STMP. Overall, the nature of the species present was the same in each sample, but at higher concentrations of STMP, larger amounts of inorganic species were present.

It was important to note that while the locations of the peaks generally corresponded to those seen in literature (e.g. triphosphates *vs.* monophosphates),[81,82] absolute assignments proved difficult due to the wide range of possibilities and the small differences in chemical shift between certain organophosphate species (e.g. phosphodiesters *vs.* monophosphates). Furthermore, chemical shifts may differ depending on which hydroxyl group in the sugar ring the phosphate species was bound to. To resolve these peaks definitively, it may be necessary to be break down the STMP-SNPs into smaller macromolecules by using enzymes (such as amylase) and performing ^{31}P- NMR again. This would sharpen each individual peaks to a point where assignment could be possible.

2.2.7 Water Retention of Nanogels

One interesting property of the prepared nanogels is their ability to retain water and swell, much like a macroscopic gel. In typical crosslinked nanogels, the degree of swelling is inversely proportional to the degree of crosslinking; a higher crosslinking density prevents the polymer chains from expanding in water.[124,125] A plot of STMP concentration *vs.* mass of water retained, as well as an iodine stain of the swollen gel is shown in Figure 20 A) and B) respectively. Surprisingly, a significant amount of water was only retained at very high STMP concentration. Despite TEM images clearly showing crosslinked particles at lower concentrations of STMP (more specifically, 5 and 10 mol% STMP), very little water retention was observed. A possible explanation for this could lie in the inefficiency of the crosslinking reaction itself. As evident from NMR, apart from peaks attributed to crosslinking, there is a much higher degree of triphosphates present. It is known that the presence of charged groups within a crosslinked network can contribute to swelling through electrostatic repulsion.[126–128]At

higher concentrations of STMP, the increase in organic triphosphates could induce significant electrostatic repulsion within the STMP-SNPs, leading to a higher degree of swelling. However, these triphosphates were not as present at low STMP concentrations (relative to monophosphates and phosphodiesters). As a result, there is less swelling at lower concentrations.

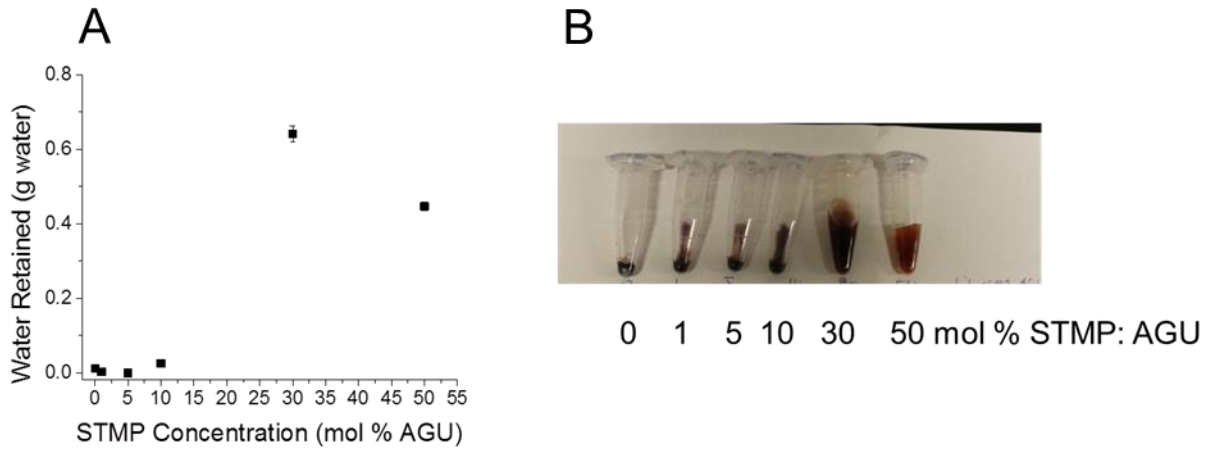

Figure 20. Mass of water retained in nanogels prepared at different STMP concentrations (A) and iodine stained gels of the centrifuged product (B). In general, there was very little water retention at low STMP concentrations, with a significant increase at 30 mol %.

To further investigate the nature of swelling of the nanogels, the effect of salt on the water retention of the 30 mol% STMP-SNP sample was tested. Salts can screen the electrostatic repulsion within the polymer network, and potentially decrease swelling. The water retention as a function of salt concentration, as well as an iodine-stained image of the centrifuged 30 mol % STMP-SNPs as a function of NaCl concentration is shown in Figure 21 A) and B) respectively. For both salts, there was a significant decrease in the amount of water retained by the gel. This decrease was more gradual with NaCl compared to $MgCl_2$, likely reflecting the fact that Mg^{2+} is a divalent ion and would more effectively screen the electrostatic repulsion than Na^{+}. Interestingly, the swelling was not completely prevented; about 0.2 g of water was still retained

at high concentrations of both salts. It would be unlikely for complete dehydration of the gel to occur, especially to ensure that the ions stay within the polymeric nanogel.

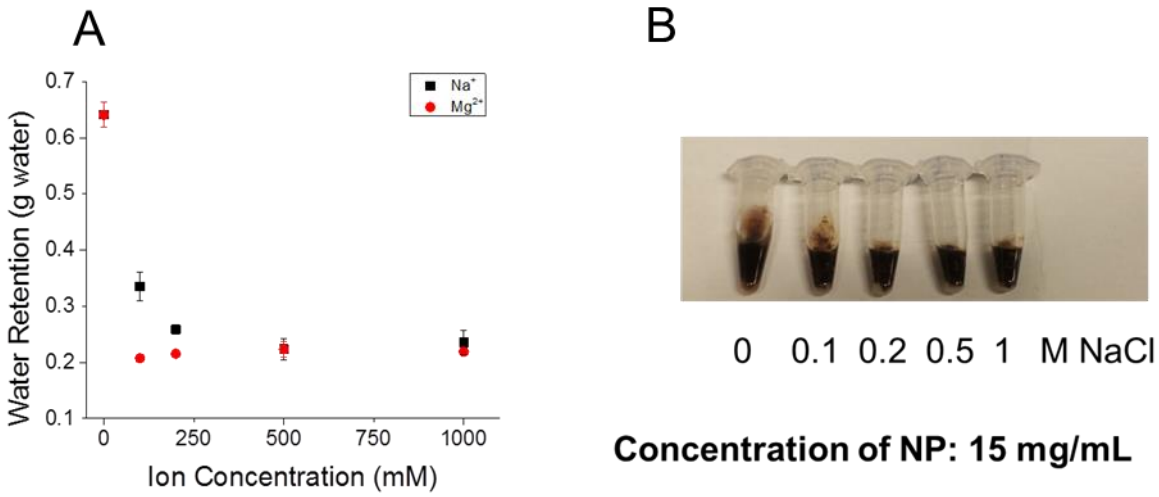

Figure 21. Mass of water retained by the 30 mol % nanogel as a function of salt concentration (A) and an image of the iodine-stained product with increasing NaCl concentration after centrifugation (B). The increase in salt concentration dramatically decreases the amount of water retained, with Mg^{2+} being more effective than Na^{+}.

2.3 Conclusion

The PIE process to make STMP-SNPs was successful based on the several characterization techniques performed. Firstly, the synthetic concept of phase inversion was confirmed from conductivity measurements, which showed a decrease in conductivity, and a corresponding decrease in droplet size. Once particles were purified and dried, the particle size and morphology varied with the amount of STMP used in the synthesis, from fibrous structures at low STMP concentration to clearly-defined internally-crosslinked nanoparticles at concentrations higher than 5 mol%. As a result, it was more accurate to call the STMP-SNPs "nanogels", as opposed to a solid particle. In general, the particle size and negative charge

increased with increasing amounts of STMP, as evident from DLS and ζ-potential. From TEM, the crosslinked chains were clearly visible within the densely-crosslinked core. The phosphorylation of the samples was confirmed by ^{31}P NMR, showing various species present after purification. This being said, individual peaks were not assigned as there were many potential possibilities. Therefore, further ^{31}P NMR work needs to be done (such as spiking experiments and enzymatic digestion) to resolve these peaks and definitively assign them. Finally, the nanogels displayed swelling behaviour; a significant amount of water was retained upon dissolution. In general, the water retained was very low when <10 mol% STMP was used. It was high at 30 mol% STMP, with 50 mol% being slightly lower. This was potentially due, in part, to influence from very charged phosphate groups, causing the internal phosphates to repel each other, leading to increased swelling. These large phosphate groups were present in greater amounts at higher STMP concentration. Another potential explanation lay in the inefficiency of the crosslinking reaction itself; only STMP concentrations higher than 10 mol% could induce significant crosslinking, which was reflected in the swelling characteristics. Increasing salt concentration also resulted in a lower amount of water retained likely due to screening of this electrostatic repulsion. While there was extensive characterization performed, more techniques (such as viscosity measurements) will need to be done in the future to further understand the nature of the nanogels.

Chapter 3. Drug Delivery Studies

3.0 Introduction

After successful preparation and characterization of phosphate crosslinked nanoparticles, the potential application in drug delivery was explored. For this purpose, confirmation was needed that the nanoparticles were biocompatible (not toxic to cells). This was done using an MTT assay. An MTT assay is normally used to determine *in-vitro* cell viability/toxicity. The MTT reagent, 3-(4,5-dimethylthiazol-2-yl)-2,5-diphenyltetrazolium, is internalized by live cells and converted to a formazan by oxidoreductase enzymes, which has a strong purple colour.[129] This purple colour could be quantified by absorbance at 570 nm. A strong purple colour indicates no cell toxicity, while a non-existent purple colour indicates high toxicity. In addition, another aspect of drug delivery is the ability of the nanoparticle to load and release drug. Since the linkage formed between the starch chains is negatively-charged (due to the phosphate group), there was an inherent limitation on the types of drugs that could be loaded within the crosslinked starched network. For example, hydrophobic drugs like docetaxel were unlikely to partition into the porous structure and instead precipitate out as free docetaxel. However, a positively charged drug (such as doxorubicin, with pK_a=9.53[130]), would preferentially partition into these pores and load effectively. In addition, doxorubicin (DOX) is fluorescent ($\lambda_{excitation}$=490 nm, $\lambda_{emission-}$=590nm), and quantification of the release could be done using fluorescence-based assays.

3.1 Materials and Methods

MTT Assay. Typically, HeLa cells were seeded into 60 wells of a 96 well plate at a concentration of 5000 cells/well and left to proliferate (grow and divide) overnight. The next

day, the sample was washed with phosphate-buffered saline (PBS) and 100 μL of cell medium was added. At this time, 100 μL of 10 mg/mL 0 mol% STMP and 30 mol% STMP samples were added to the first well (final concentration 5 mg/mL) and a serial dilution was performed so that the next well was half the concentration of the previous well. In other words, the most concentrated well was 5 mg/mL, followed by the next well which was 2.5 mg/mL, and this dilution continued until well 9. Well 10 was reserved as a control for no sample. Since the assay was run in triplicates, each sample would be allocated 30 wells (10 for each series with 2 duplicates). The cells were left to incubate with the sample overnight. The next day, 25 μL of 5 mg/mL MTT reagent was added and allowed to be internalized into the cells for 2 hours. The cells were then lysed (broken apart) by pH 4.7 dimethyl sulfoxide (DMSO) to release and dissolve the purple formazan created in the cells. After 4 hours of incubation, the absorbance at 570 nm was measured using a SpectraMax M3 spectrometer. The cell viability was calculated according the following equation:

$$Cell\ Viability\ (\%) = \frac{A_{sample}}{A_{control}} * 100\%$$

Where A_{Sample} was the measured absorbance of the sample well and $A_{control}$ was the measured absorbance of the control well (without any sample).

DOX Calibration Curve. From a stock DOX solution of 1 mg/mL in water, several dilutions were made so that a final concentration of 5 μg/mL was reached. The fluorescence of this solution was measured using a Varian spectrometer using an excitation wavelength of 490 nm and observing the emission peak at 590 nm. A calibration curve was generated using 5 μg/mL as the highest concentration to 0.01 μg/mL as the lowest. A fit of the plot was found using linear interpolation constraining the intercept to 0.

Drug Loading. In a typical loading experiment, 100 μg of DOX was mixed 100 μg of STMP-SNPs in 1 mL of 50 mM buffer and incubated for 4 hours. After incubation, the samples were centrifuged to separate bound drug from loaded drug. The fluorescence of the supernatant at 590 nm was measured using fluorescence spectroscopy using an excitation wavelength of 490 nm. The drug loading capacity was then calculated according to the following equation

$$Loading\ Capacity\ (\%) = \frac{D - \frac{F}{S}}{D} * 100\%$$

Where D was the total drug added (in all cases 100 μg), F was the fluorescence of the free drug measured after centrifugation, and S was the slope of the calibration curve within the range of detection (12.454 a.u./ (μg/mL)).

Drug Release. For drug release, STMP-SNPs were loaded at the optimal conditions determined from previous experiments, dispersed in 1 mL of 50 mM buffer, and placed within a 3500 Da molecular weight cut-off dialysis membrane. The sample was then dialyzed against 19 mL of a 50 mM buffer (Total volume= 20 mL). The fluorescence of the dialysate was measured using fluorescence spectroscopy. The released drug was calculated according to the following equation:

$$Release\ (\%) = \frac{F}{L * S} * X * 100\%$$

Where F was the fluorescence intensity of the dialysate (a.u.), L was the loaded drug concentration (μg/mL), S was the slope (12.454 a.u./(μg/mL)), and X was the dilution factor due to the volume of dialysate (20).

Drug Release in Culture Environments. The 30 mol% STMP-SNPs (100 μg) were loaded with DOX to capacity in 1 mL 50 mM pH 7.6 HEPES buffer, washed three times with water and finally redispersed in 1 mL PBS, DMEM, 10% FBS and 100% FBS, before leaving to mix. The samples were centrifuged at the required time point and 10 μL of the supernatant was diluted to 590 μL of PBS for measurement in a Varian fluorescence spectrometer. Using the calibration curve, released DOX was calculated using the following equation:

$$DOX\ Released\ (\%) = \frac{F}{S * L}$$

Where F was the fluorescence of the supernatant measured by spectroscopy (a.u.), S was the slope of the calibration curve (a.u./(μg/mL) and L was the loaded drug concentration (for 30 mol% STMP-SNP: 40 μg/mL).

3.2 Results and Discussion

3.2.1 MTT Assay

As mentioned previously, the MTT assay was used to determine if the synthesized particles were toxic by themselves to the cancer cells. The cell viability plots for both the 0 mol% and 30 mol% STMP samples are shown in Figure 22. Overall, there was very little toxicity seen in both samples. Though there was a noticeable decrease in the viability at 2.5 and 5 mg/mL for the 30 mol% sample, this was also seen in the 0 mol% sample. This suggested that either starch itself was toxic beyond 2.5 mg/mL (though this was unlikely due to the fact that this was studied with BLNPs previously) or there may have been some chemicals (oil or surfactant)

which may not have been removed during the purification process. Another potential reason was the dilution of the cell medium at very high concentrations. Due to use of serial dilutions, the well containing the highest concentration of sample would have the lowest concentration of medium. This could have affected the rate of cell proliferation. In any case, this effect was not very pronounced and only small decreases in the cell viability were noted. Furthermore, a concentration of 2.5 mg/mL is already quite high for clinical applications. While many data points showed that there seemed to be increased cell proliferation at low concentration of sample, the wide error bars suggested that this effect may be due to the natural variation of cell proliferation in a specific well.

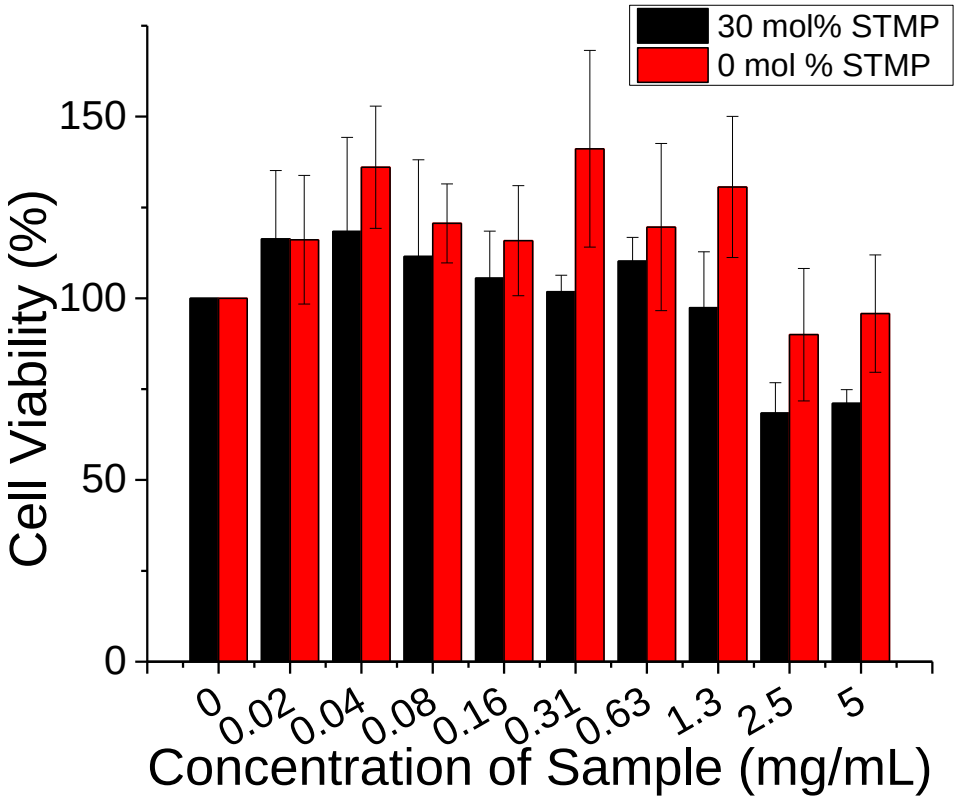

Figure 22. MTT Assay for 0 mol% and 30 mol% samples with HeLa cells.

3.2.2 Drug Loading and Release

Before any drug loading experiments were performed with prepared STMP-SNPs, a calibration curve for free DOX was generated as shown in Figure 23, showing the fluorescence intensity as a function of DOX concentration. In addition to being fluorescent, DOX is also quite coloured; at higher concentrations, inner filter effects affected the linearity of the calibration curve. As such, a linear fit could only be found from 0 μg/mL to 5 μg/mL.

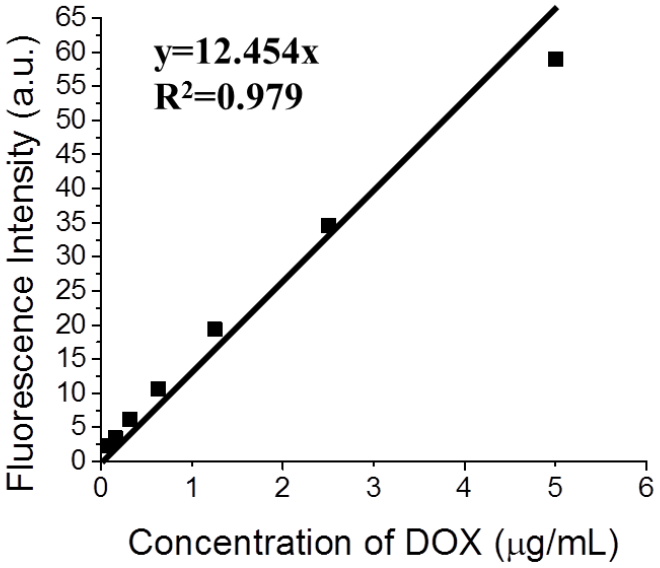

Figure 23. Calibration curve for DOX found by fluorescence spectroscopy.

DOX is water-soluble, implying that if there is no loading, the drug would remain in the supernatant after centrifugation while the nanoparticles settle to the bottom. The drug loading for STMP-SNP samples prepared with 30 mol % STMP was determined at different pH as shown in Figure 24 A. The buffers used were: 50 mM HEPES (pH 7.6), 50 mM citrate (pH 6), 50 mM acetate (pH 4). Drug loading was nearly 4-fold higher at pH 7.6 compared to pH 4 or 6. This was

likely due to the fact that there were more phosphate groups deprotonated at higher pH, giving the STMP-SNPs a more negative charge. The pk_a of DOX (9.53) ensures that the drug is also quite positively charged. This means that electrostatic interactions are stronger between the DOX and the STMP-SNPs at higher pH, resulting in a higher loading. At lower pH, drug loading is limited as most phosphate groups would be protonated with the exception of the phosphodiester and monophosphate species. It can be concluded, therefore, that the presence of larger phosphate species (such as diphosphates and triphosphates) provides significant contributions to the drug loading. At pH 7.6, the loading capacity achieved was ~40%. This meant that for 100 μg of SNP, 40 μg of DOX was bound. Compared to the previously-studied TEMPO-oxidized BLNPs, where the loading capacity was 0.05%, this represented a ~800-fold improvement in loading capacity. This could be attributed to the larger size of the nanoparticles, as well as the introduction of highly negatively charged phosphate groups which aid in the drug binding.

Once the optimal drug loading pH was known, drug was loaded on to the starch nanoparticles at pH 7.6, followed by release studies using dialysis at different pH. The release profiles for this experiment are shown in Figure 24 B. Within the first 1-2 days for all three samples, there is a sharp release of drug from the nanoparticle which could be due to drug that is more loosely bound or due to the sharp concentration gradient between the dialysate and the sample. Beyond this, the released drug increases slowly with time reflecting the diffusion of the more tightly-bound drug. The amount of drug released was significantly greater at lower pH compared to that the loading pH. This could also be explained by the weaker electrostatic interactions between the drug and the STMP-SNP, as discussed previously. This release at lower pH was extremely desirable for drug delivery applications, as cancer cell interiors tend to be

more acidic than physiological pH. Therefore, internalization of the loaded STMP-SNPs would lead to a significant "burst" release in cells.

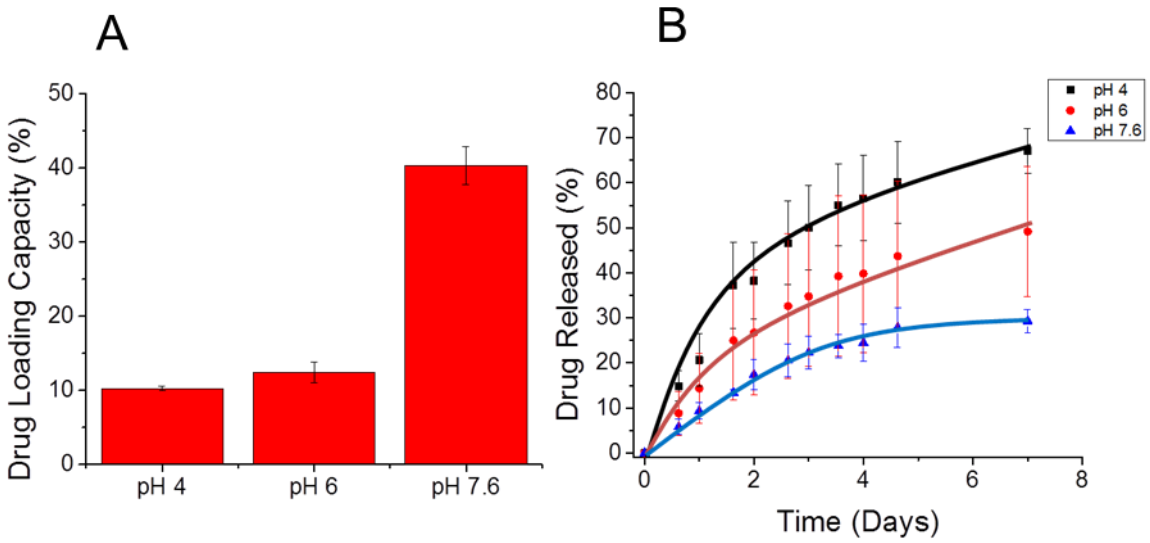

Figure 24. Drug loading capacity of 30 mol% STMP-SNPs with pH (A) and drug release profiles of the same sample at different pH (B). For the release profile, the drug was loaded at pH 7.6.

Next, the effect of STMP concentration used in the synthesis on the drug loading and release profiles was investigated. Evident from NMR, there is a higher amount of triphosphates at 30 and 50 mol% STMP relative to monophosphates compared to lower concentrations where monophosphates and phosphodiester linkages dominate. The drug loading capacities in 50 mM HEPES buffer at pH 7.6 for the various STMP-SNPs are shown in Figure 25 A. In general, the loading capacity increases with STMP content until 30 mol %, with a slight decrease thereafter. The increase in drug loading capacity is attributed to a higher concentration of phosphate species (especially di- and tri- phosphates) within the crosslinked nanoparticle. However, the decrease with the 50 mol % sample went against the trend. Since there were more available phosphates, there should have been a higher drug loading capacity if the drug loading was purely electrostatic in nature. An interesting comparison for this drug loading data was the swelling studies

previously performed. It was seen that with 50 mol % STMP, there was slightly less water retained in the nanogel compared to 30 mol %. It was quite possible that, in addition to electrostatic interactions, there was also significant influence from the volume of the nanoparticle to "store" the drug on the overall drug loading. It would also explain why there is a large jump in the capacity between 10 and 30 mol % STMP.

The release of the loaded STMP-SNPs at different STMP concentrations was monitored at pH 4 and the profile is shown in Figure 25 B. The sample prepared without STMP showed a complete burst release, implying that the drug was only loosely bound to this material. All samples prepared with STMP had a much more gradual release, indicating stronger drug/SNP interactions. There was no obvious trend in the release profile with STMP concentration. A minimum of drug was released (relative to the loaded drug) at 10 mol % STMP as compared to 30 or 50 mol%, where a higher percentage was released. One possible explanation is the protonation of the triphosphates and diphosphates at low pH. From ^{31}P-NMR, it was evident that there was an abundance of larger organic phosphates which contributed to the high loading, as discussed previously. However, in terms of release, the protonation of these groups created a large concentration gradient of free drug from inside and outside the dialysis membrane, resulting in more drug released. At low STMP concentrations, there likely were more monophosphates/phosphodiester linkages (relative to larger phosphate species) which bound less DOX, but were not deprotonated at low pH. Therefore, a lower percentage of DOX was released.

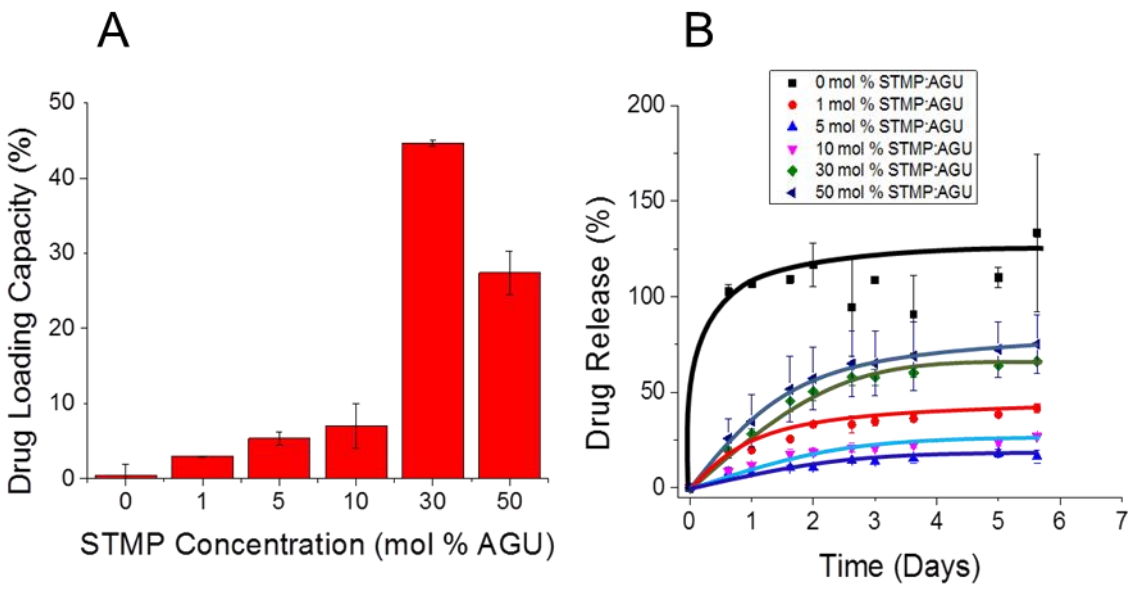

Figure 25. Drug loading capacity at pH 7.6 for STMP-SNPs prepared at different concentrations of STMP (A) and release profiles of these loaded STMP-SNPs at pH 4 (B).

Finally, to investigate the effect of cell culture environment on the drug release, the loaded STMP-SNPs were placed in various environments. These included phosphate-buffered saline (PBS), Dulbecco's Modified Eagle Medium (DMEM), 10% Fetal Bovine Serum (FBS) in DMEM, and 100% FBS. PBS is typically used as a sodium phosphate buffer formulation containing various salts to match physiological ion concentration, as well as pH found in blood. DMEM is the typical medium used for culturing many cell lines (including cancer cells) and contains vitamins, glucose and essential amino acids for cell growth and proliferation. FBS is the supernatant of centrifuged blood of a bovine fetus after adding a coagulant. This normally contains several proteins typically found in human blood, a major component of which is bovine serum albumin (BSA).

The DOX release in these environments at 2 and 36 hours after redispersion are shown in Figure 26. Even for PBS, significant desorption of drug was seen after just 2 hours, even though the pH of this buffer was 7.4. This could be attributed to the high salt concentration (>100 mM)

which may have screened the attractive electrostatic interactions between the SNPs and the drug. In addition, the presence of the phosphates in the buffer may have attracted bound drug from the SNPs to the free solution. There was no major difference in the released drug after 2 hours across all the environments studied with ~30% of the drug released on average. After 36 hours, the sample incubated in 100% FBS showed complete desorption of DOX, whereas PBS had released ~60 % of the loaded DOX. Many of the proteins in the FBS likely contain positively charged residues (e.g. lysine or arginine) which could effectively displace the doxorubicin from the SNPs. However, this likely required more time due to the proteins being more bulky than the salts in PBS and subsequently, steric hindrance slowed the adsorption of the proteins to the SNPs.

In an ideal case, the drug would be adsorbed within the network of the STMP-SNPs such that larger macromolecules (such as proteins) would not be able to penetrate and displace it. However, it appeared that the pore size of the nanogel permitted these larger molecules to diffuse in, affecting the drug release. Another potential explanation was that most of the DOX was adsorbed only on the surface of the STMP-SNP (and not within the crosslinked network). Therefore, it would be much easier for the aforementioned molecules to disrupt the adsorption.

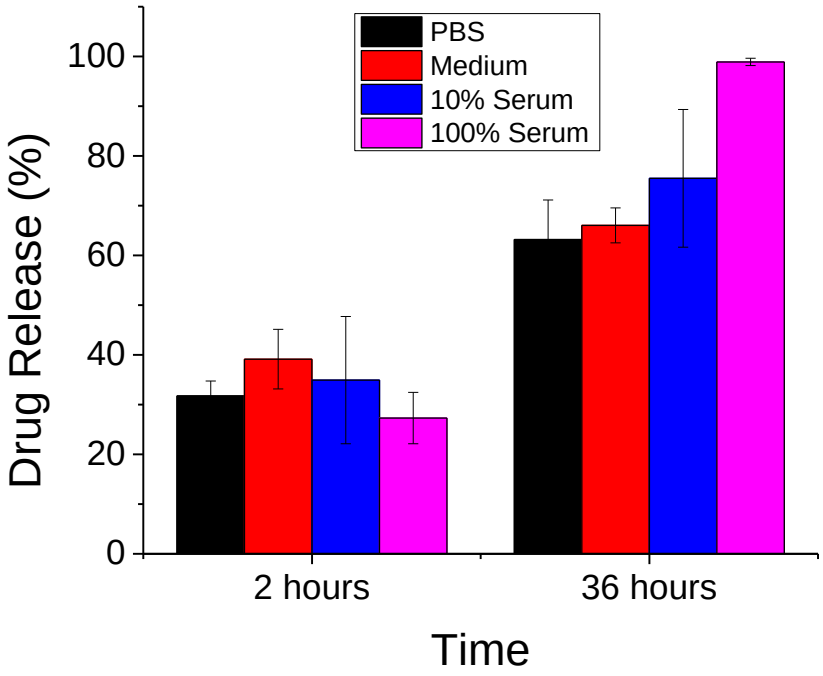

Figure 26. Drug release in various cell culture environments. The release was much more apparent in these mixtures compared to a simple buffer.

3.3 Conclusion

In general, the prepared STMP-SNPs were non-toxic as seen from the MTT assay. Any small deviation from the control did not show any specific trend, implying that the differences were likely due to natural variation in cell proliferation rates. This being said, a small decrease in cell viability was seen in both the 0 mol % and 30 mol% STMP-SNPs. This was potentially due to residual impurities from the PIE process or dilution of the cell medium at higher sample concentrations.

Drug loading and release experiments conducted in simple environments (only buffer) showed significant promise. More specifically, loading capacity for the 30 mol% STMP-SNPs at

pH 7.6 was 40%, representing an 800-fold improvement over the BLNPs previously studied. In addition, the release was accelerated at lower pH, which was more desirable as cancer cell environments are more acidic than physiological conditions. Generally, there was increase in drug loading with STMP concentration used to prepare the nanogels. This reaches a maximum at 30 mol % (~40% loading), tapering off slightly with 50 mol % (~30% loading). Curiously, this trend reflected the ability of the nanogels to retain water, with the highest drug loading occurring in the same sample which retained the water. This suggested that, in addition to electrostatic interactions, the swelling behaviour also influenced the drug loading within the STMP-SNPs. However, when loaded STMP-SNPs were placed in more typical cell culture environments, drug release was much quicker. It was likely that increased salt concentration, and the presence of proteins/other interferences caused the adsorbed drug to desorb from the nanoparticles. This essentially limits the nanogel usage for drug delivery applications.

Chapter 4. Conclusions and Future Work

Nanoparticles have considerable potential in drug delivery applications. Some have already been implemented in a clinical setting (such as liposomes), while others have regulatory hurdles to cross and many are still in the early stages of investigation. Experimental grade BLNPs were previously provided by EcoSynthetix, a collaborating company on this project, to explore such applications, using DNA as an active targeting agent. In those studies it was found that these nanoparticles were too small; DNA aptamer coverage was scarce (resulting in low cellular uptake) and the drug loading was very low. Consequently, it was decided to use a food-grade crosslinker, STMP, to increase the size of the nanoparticles through the formation of covalent phosphate crosslinks. The challenge lay in confining the particle size so that this process was not completed in bulk. To do this, an emulsion based protocol was followed based on a patent held by the collaborating company. In brief, a phase inversion emulsion allowed for sufficiently small droplet size to be formed using high shear mixing.

The phosphate-crosslinked SNPS (STMP-SNPs) were successfully prepared using different amounts of STMP during the crosslinking process. They were characterized using TEM, DLS and SEM. In general, the particle size increased with increasing STMP concentration, with more obvious nanoparticles observed at STMP concentrations higher than 5 mol %. The STMP-SNPs were negatively charged due to phosphorylation, while the sample prepared without STMP was neutral, as measured from ζ-potential. The particle morphology, with interconnected regions of crosslinked chains suggested that these were nanogels, rather than solid particles. ^{31}P NMR was performed on the STMP-SNPs and in general, many different organic phosphorus species, such as monophosphates and diphosphates, were present along with the phosphodiester linkages. However, enzymatic digestion of the STMP-SNPs may be

necessary in order to definitively resolve the peaks obtained from the spectra as significant broadening was present. At high STMP concentrations, the prepared nanogels retained significant amounts of water. This was due, in part, to the electrostatic repulsion of the larger phosphate species within the crosslinked polymer network. Confirmation of this electrostatic repulsion mechanism was found from the addition of salt to the nanogels, which significantly reduced the amount of water retained.

Finally, the performance of the STMP-SNPs as a drug delivery vehicle was explored. Firstly, an MTT assay was used to determine any toxicity to the HeLa cancer cell line. It was found that the samples containing STMP did not show any significant toxicity as compared to the sample without STMP. For both samples, toxicity seemed to increase at 2.5 mg/mL but may likely have been due to either impurities from the emulsion process or medium dilution. The drug loading studies indicated that the model drug, DOX, was optimally adsorbed on to the STMP-SNPs at pH 7.6, and the loading capacity was 800-fold higher than previously-studied BLNPs. The release of the drug from the STMP-SNPs was much quicker at lower pH, likely reflecting the protonation of the phosphate species in a more acidic environment. It was also seen that the STMP-SNPs prepared with 30 mol% STMP had the highest drug loading, which likely reflected the swelling behaviour of this particular sample.

4.1 Future Work

In terms of synthesis, it appeared that a large amount of STMP was necessary to observe any significant particle formation. Ideally, a low amount would be necessary; it would be easier to purify, as well as being more cost-effective. One potential way to improve the crosslinking

would be to add a divalent (or event trivalent) metal ion, in addition to the NaCl used in the study, as a catalyst during the PIE process.

While extensive characterization was carried out, there remains some potential work to be done to fully understand the nature of the material. Firstly, viscosity measurements should be performed on the prepared samples to determine both molecular weight and the swell ratio. Ideally, the molecular weights of the STMP-SNPs would be higher than the BLNPs, as well as the sample prepared without STMP. The swell ratio could be used as evidence of crosslinking, with lower swell ratios corresponding to a higher crosslinking density. However, based on water retention studies, this may not necessarily be the case. Rheological experiments could also be conducted on the STMP-SNPs to determine the crosslinking density through measurement of the storage moduli. Finally, for an in-depth picture of the composition of the STMP-SNPs, enzymatic digestion should be performed to break down the high molecular weight particle into phosphorylated oligomers. This would significantly help ^{31}P NMR studies and resolve broadened peaks for proper assignment. Since ^{31}P NMR as performed was not quantitative, other methods could be used to determine the amount of phosphorus in the sample, such as inductive-coupled plasma (ICP) elemental analysis.

With regards to drug delivery applications, the current study suggests that DOX-loaded STMP-SNPs are very susceptible to drug release under typical cell culture environments. If this were due to simple surface attachment of the DOX to the STMP-SNPs, the problem could be solved by incorporating the DOX during the PIE process to ensure that it would be internalized in the nanogel structure.

Finally, once the STMP-SNPs have been fully characterized, its cellular uptake could be explored. TEMPO-mediated oxidation or other methods (such as using trichloroacetate) could be used to convert hydroxyl groups on the STMP-SNP to carboxyl groups. Following this, EDC/NHS coupling could be used to conjugate dye-labelled DNA aptamer or free dyes to the surface of the nanogel to observe its internalization in cancer cells.

Letter of Copyright Permission

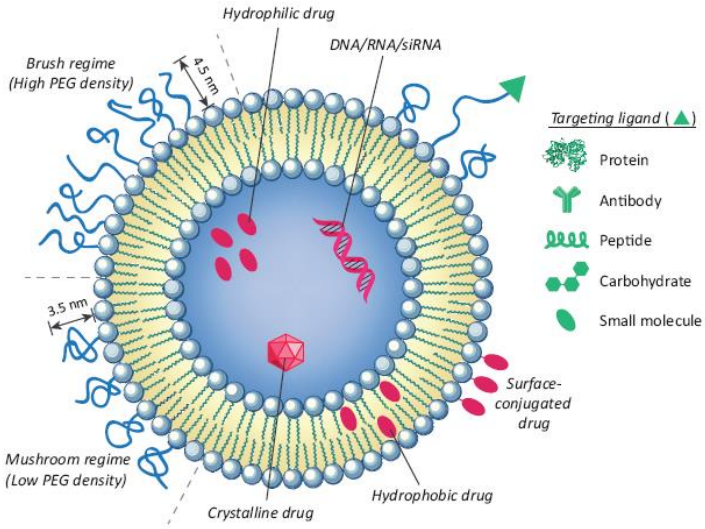

Title of Article: Liposomes as Potential Drug Carrier Systems for Drug Delivery

Çağdaş, M.; Sezer, A. D.; Bucak, S. In Application of Nanotechnology in Drug Delivery; Sezer, A. D., Ed.; InTech, 2014.

Figure: 1

Authors: Melis Çağdaş, Ali Demir Sezer and Seyda Bucak

Source: http://www.intechopen.com/books/application-of-nanotechnology-in-drug-delivery/liposomes-as-potential-drug-carrier-systems-for-drug-delivery

License: Creative Commons 3.0 (https://creativecommons.org/licenses/by/3.0/legalcode)

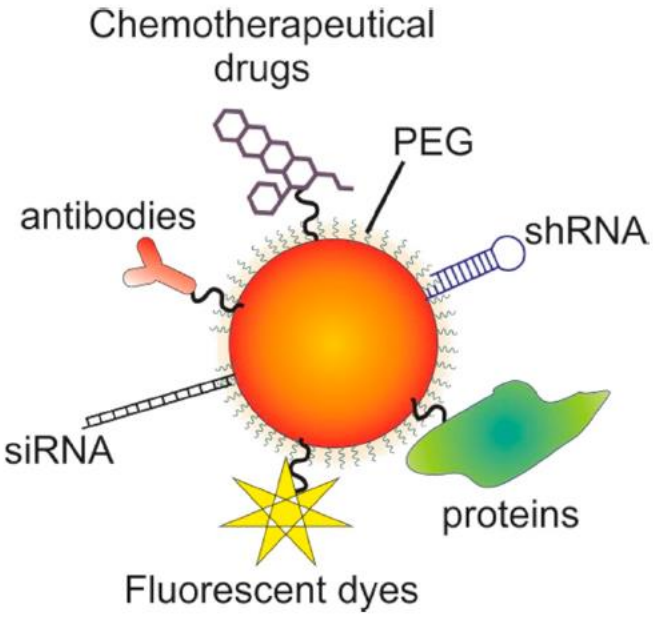

Title of Article: Tumor Microenvironment Modulation via Gold Nanoparticles Targeting Malicious Exosomes: Implications for Cancer Diagnostics and Therapy

Roma-Rodrigues, C.; Raposo, L. R.; Cabral, R.; Paradinha, F.; Baptista, P. V.; Fernandes, A. R. Int. J. Mol. Sci. 2017, 18 (1), 162.

Figure: 4

Authors: Catarina Roma-Rodrigues, Luís R. Raposo, Rita Cabral, Fabiana Paradinha, Pedro V. Baptista and Alexandra R. Fernandes

Source: http://www.mdpi.com/1422-0067/18/1/162

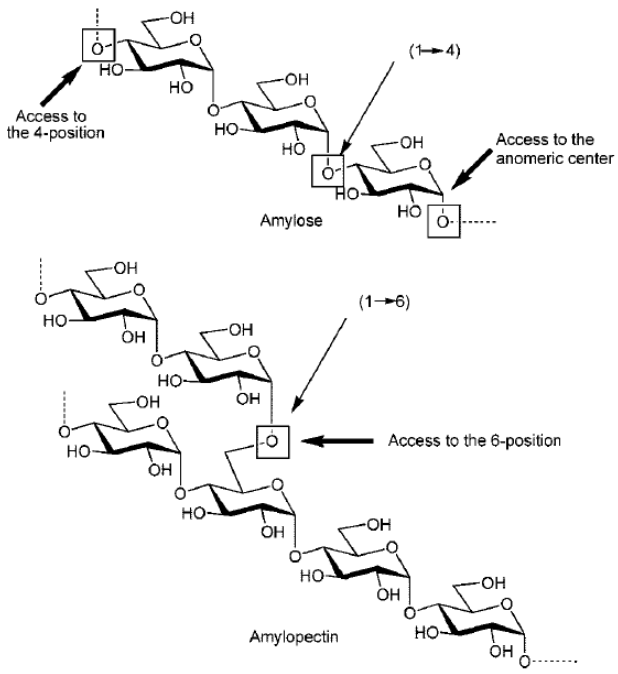

Title of Article: First Principles Insight into the α-Glucan Structures of Starch: Their Synthesis, Conformation, and Hydration

Damager, I.; Engelsen, S. B.; Blennow, A.; Lindberg Møller, B.; Motawia, M. S. Chem. Rev. 2010, 110 (4), 2049–2080

Figure: 23

Authors: Iben Damager, Søren Balling Engelsen, Andreas Blennow, Birger Lindberg Møller and Mohammed Saddik Motawia

Source: http://pubs.acs.org/doi/abs/10.1021/cr900227t

License: Standard ACS AuthorChoice (http://pubs.acs.org/page/policy/authorchoice_termsofuse.html)

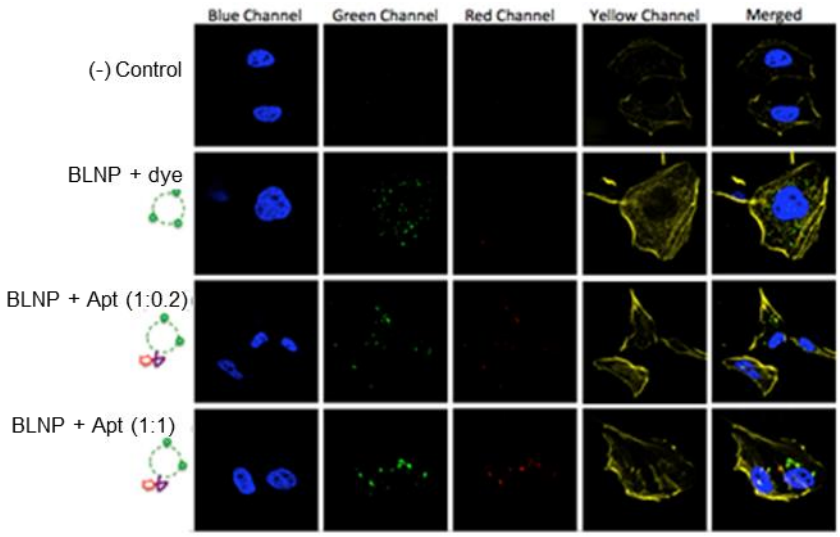

Title of Article: Starch Nanoparticles for Targeted Anti-Cancer Drug Delivery

Tsung Hao Tsai (2015). UWSpace

Figure: 30

Authors: Tsung Hao Tsai

Source: http://hdl.handle.net/10012/9573

License: Permission by author

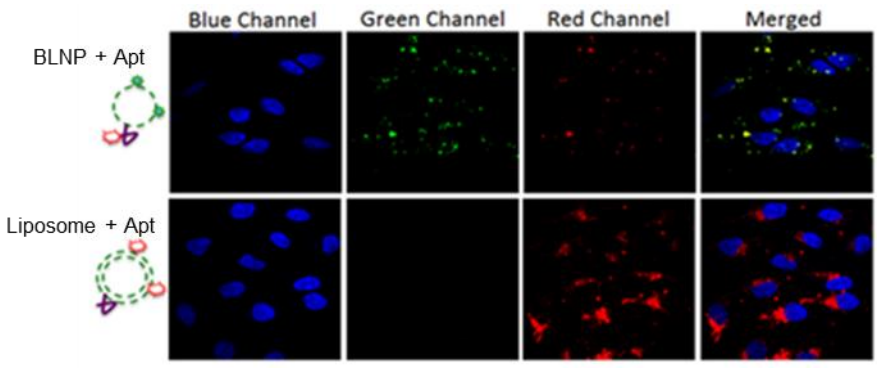

Title of Article: Starch Nanoparticles for Targeted Anti-Cancer Drug Delivery

Tsung Hao Tsai (2015). UWSpace

Figure: 32

Authors: Tsung Hao Tsai

Source: http://hdl.handle.net/10012/9573

License: Permission by author

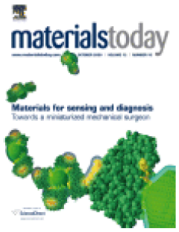

Title: Carbon materials for drug delivery & cancer therapy

Author: Zhuang Liu,Joshua T. Robinson,Scott M. Tabakman,Kai Yang,Hongjie Dai

Publication: Materials Today

Publisher: Elsevier

Date: July–August 2011

Order Completed

Thank you for your order.

This Agreement between Anand Lopez ("You") and Elsevier ("Elsevier") consists of your license details and the terms and conditions provided by Elsevier and Copyright Clearance Center.

Your confirmation email will contain your order number for future reference.

Printable details.

License Number	4074980144636
License date	Mar 23, 2017
Licensed Content Publisher	Elsevier
Licensed Content Publication	Materials Today
Licensed Content Title	Carbon materials for drug delivery & cancer therapy
Licensed Content Author	Zhuang Liu,Joshua T. Robinson,Scott M. Tabakman,Kai Yang,Hongjie Dai
Licensed Content Date	July–August 2011
Licensed Content Volume	14
Licensed Content Issue	7-8
Licensed Content Pages	8
Type of Use	reuse in a thesis/dissertation
Portion	figures/tables/illustrations
Number of figures/tables/illustrations	1
Format	both print and electronic
Are you the author of this Elsevier article?	No
Will you be translating?	No
Order reference number	
Original figure numbers	1
Title of your thesis/dissertation	Synthesis of Phosphate Crosslinked Starch Nanoparticles for Drug Delivery
Expected completion date	Apr 2017
Estimated size (number of pages)	80
Elsevier VAT number	GB 494 6272 12
Requestor Location	Anand Lopez 27 Elgin Street Waterloo, ON N2J 2P9 Canada Attn: Anand Lopez
Total	0.00 CAD

ORDER MORE CLOSE WINDOW

Title:	Biomaterials for promoting brain protection, repair and regeneration
Author:	Gorka Orive, Eduardo Anitua, Jose Luis Pedraz and Dwaine F. Emerich
Publication:	Nature Reviews Neuroscience
Publisher:	Nature Publishing Group
Date:	Sep 1, 2009

Order Completed

Thank you for your order.

This Agreement between Anand Lopez ("You") and Nature Publishing Group ("Nature Publishing Group") consists of your license details and the terms and conditions provided by Nature Publishing Group and Copyright Clearance Center.

Your confirmation email will contain your order number for future reference.

Printable details.

License Number	4074980322843
License date	Mar 23, 2017
Licensed Content Publisher	Nature Publishing Group
Licensed Content Publication	Nature Reviews Neuroscience
Licensed Content Title	Biomaterials for promoting brain protection, repair and regeneration
Licensed Content Author	Gorka Orive, Eduardo Anitua, Jose Luis Pedraz and Dwaine F. Emerich
Licensed Content Date	Sep 1, 2009
Licensed Content Volume	10
Licensed Content Issue	9
Type of Use	reuse in a dissertation / thesis
Requestor type	academic/educational
Format	print and electronic
Portion	figures/tables/illustrations
Number of figures/tables/illustrations	1
High-res required	no
Figures	Figure 2 a
Author of this NPG article	no
Your reference number	
Title of your thesis / dissertation	Synthesis of Phosphate Crosslinked Starch Nanoparticles for Drug Delivery
Expected completion date	Apr 2017
Estimated size (number of pages)	80
Requestor Location	Anand Lopez 27 Elgin Street Waterloo, ON N2J 2P9 Canada Attn: Anand Lopez
Billing Type	Invoice
Billing address	Anand Lopez

RightsLink®

Home | Account Info | Help

RSC Publishing

Title:	Liposome-like nanostructures for drug delivery	Logged in as: Anand Lopez
Author:	Weiwei Gao,Che-Ming J. Hu,Ronnie H. Fang,Liangfang Zhang	LOGOUT
Publication:	Journal of Materials Chemistry B	
Publisher:	Royal Society of Chemistry	
Date:	Oct 9, 2013	

Order Completed

Thank you for your order.

This Agreement between Anand Lopez ("You") and Royal Society of Chemistry ("Royal Society of Chemistry") consists of your license details and the terms and conditions provided by Royal Society of Chemistry and Copyright Clearance Center.

Your confirmation email will contain your order number for future reference.

Printable details.

License Number	4074980433395
License date	Mar 23, 2017
Licensed Content Publisher	Royal Society of Chemistry
Licensed Content Publication	Journal of Materials Chemistry B
Licensed Content Title	Liposome-like nanostructures for drug delivery
Licensed Content Author	Weiwei Gao,Che-Ming J. Hu,Ronnie H. Fang,Liangfang Zhang
Licensed Content Date	Oct 9, 2013
Licensed Content Volume	1
Licensed Content Issue	48
Type of Use	Thesis/Dissertation
Requestor type	academic/educational
Portion	figures/tables/images
Number of figures/tables/images	1
Distribution quantity	4
Format	print and electronic
Will you be translating?	no
Order reference number	
Title of the thesis/dissertation	Synthesis of Phosphate Crosslinked Starch Nanoparticles for Drug Delivery
Expected completion date	Apr 2017
Estimated size	80
Requestor Location	Anand Lopez 27 Elgin Street Waterloo, ON N2J 2P9 Canada Attn: Anand Lopez
Billing Type	Invoice
Billing address	Anand Lopez 27 Elgin Street

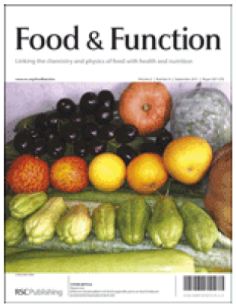

Title: Molecular disassembly of starch granules during gelatinization and its effect on starch digestibility: a review

Author: Shujun Wang,Les Copeland

Publication: Food & Function

Publisher: Royal Society of Chemistry

Date: Sep 9, 2013

Order Completed

Thank you for your order.

This Agreement between Anand Lopez ("You") and Royal Society of Chemistry ("Royal Society of Chemistry") consists of your license details and the terms and conditions provided by Royal Society of Chemistry and Copyright Clearance Center.

Your confirmation email will contain your order number for future reference.

Printable details.

License Number	4074980552968
License date	Mar 23, 2017
Licensed Content Publisher	Royal Society of Chemistry
Licensed Content Publication	Food & Function
Licensed Content Title	Molecular disassembly of starch granules during gelatinization and its effect on starch digestibility: a review
Licensed Content Author	Shujun Wang,Les Copeland
Licensed Content Date	Sep 9, 2013
Licensed Content Volume	4
Licensed Content Issue	11
Type of Use	Thesis/Dissertation
Requestor type	academic/educational
Portion	figures/tables/images
Number of figures/tables/images	1
Distribution quantity	4
Format	print and electronic
Will you be translating?	no
Order reference number	
Title of the thesis/dissertation	Synthesis of Phosphate Crosslinked Starch Nanoparticles for Drug Delivery
Expected completion date	Apr 2017
Estimated size	80
Requestor Location	Anand Lopez 27 Elgin Street Waterloo, ON N2J 2P9 Canada Attn: Anand Lopez
Billing Type	Invoice

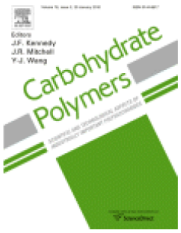

Title: Characterization of phosphorylated cross-linked resistant starch by 31P nuclear magnetic resonance (31P NMR) spectroscopy

Author: Yijun Sang,Om Prakash,Paul A. Seib

Publication: Carbohydrate Polymers

Publisher: Elsevier

Date: 22 January 2007

Order Completed

Thank you for your order.

This Agreement between Anand Lopez ("You") and Elsevier ("Elsevier") consists of your license details and the terms and conditions provided by Elsevier and Copyright Clearance Center.

Your confirmation email will contain your order number for future reference.

Printable details.

License Number	4074980693041
License date	Mar 23, 2017
Licensed Content Publisher	Elsevier
Licensed Content Publication	Carbohydrate Polymers
Licensed Content Title	Characterization of phosphorylated cross-linked resistant starch by 31P nuclear magnetic resonance (31P NMR) spectroscopy
Licensed Content Author	Yijun Sang,Om Prakash,Paul A. Seib
Licensed Content Date	22 January 2007
Licensed Content Volume	67
Licensed Content Issue	2
Licensed Content Pages	12
Type of Use	reuse in a thesis/dissertation
Portion	figures/tables/illustrations
Number of figures/tables/illustrations	1
Format	both print and electronic
Are you the author of this Elsevier article?	No
Will you be translating?	No
Order reference number	
Original figure numbers	5
Title of your thesis/dissertation	Synthesis of Phosphate Crosslinked Starch Nanoparticles for Drug Delivery
Expected completion date	Apr 2017
Estimated size (number of pages)	80
Elsevier VAT number	GB 494 6272 12
Requestor Location	Anand Lopez 27 Elgin Street Waterloo, ON N2J 2P9 Canada Attn: Anand Lopez

References

(1) WHO | Cancer http://www.who.int/mediacentre/factsheets/fs297/en/ (accessed Oct 6, 2015).
(2) Thorn, C. F.; Oshiro, C.; Marsh, S.; Hernandez-Boussard, T.; McLeod, H.; Klein, T. E.; Altman, R. B. *Pharmacogenet. Genomics* **2011**, *21* (7), 440–446.
(3) Herbst, R. S.; Khuri, F. R. *Cancer Treat. Rev.* **2003**, *29* (5), 407–415.
(4) Sun, T.; Zhang, Y. S.; Pang, B.; Hyun, D. C.; Yang, M.; Xia, Y. *Angew. Chem. Int. Ed.* **2014**, *53* (46), 12320–12364.
(5) Mitra, A.; Lee, C. H.; Cheng, K. *Advanced Drug Delivery*; John Wiley & Sons, 2013.
(6) Gregoriadis, G.; Ryman, B. E. *Biochem. J.* **1971**, *124* (5), 58P.
(7) Allen, T. M.; Cullis, P. R. *Adv. Drug Deliv. Rev.* **2013**, *65* (1), 36–48.
(8) Chang, H.-I.; Yeh, M.-K. *Int. J. Nanomedicine* **2012**, *7*, 49–60.
(9) Çağdaş, M.; Sezer, A. D.; Bucak, S. In *Application of Nanotechnology in Drug Delivery*; Sezer, A. D., Ed.; InTech, 2014.
(10) Sułkowski, W. W.; Pentak, D.; Nowak, K.; Sułkowska, A. *J. Mol. Struct.* **2005**, *744–747*, 737–747.
(11) Masayuki, Y.; Mizue, M.; Noriko, Y.; Teruo, O.; Yasuhisa, S.; Kazunori, K.; Shohei, I. *J. Controlled Release* **1990**, *11* (1), 269–278.
(12) Jhaveri, A. M.; Torchilin, V. P. *Front. Pharmacol.* **2014**, *5*.
(13) Bae, Y.; Fukushima, S.; Harada, A.; Kataoka, K. *Angew. Chem. Int. Ed.* **2003**, *42* (38), 4640–4643.
(14) Iijima, S. *Nature* **1991**, *354* (6348), 56–58.
(15) Hanene Ali-Boucetta, K. T. A.-J. *Chem. Commun. Camb. Engl.* **2008**, *4* (4), 459–461.
(16) Bianco, A.; Kostarelos, K.; Prato, M. *Curr. Opin. Chem. Biol.* **2005**, *9* (6), 674–679.
(17) Liu, Z.; Sun, X.; Nakayama-Ratchford, N.; Dai, H. *ACS Nano* **2007**, *1* (1), 50–56.
(18) Liu, J.; Cui, L.; Losic, D. *Acta Biomater.* **2013**, *9* (12), 9243–9257.
(19) Sun, X.; Liu, Z.; Welsher, K.; Robinson, J. T.; Goodwin, A.; Zaric, S.; Dai, H. *Nano Res.* **2008**, *1* (3), 203–212.
(20) Zhao, X.; Yang, L.; Li, X.; Jia, X.; Liu, L.; Zeng, J.; Guo, J.; Liu, P. *Bioconjug. Chem.* **2015**, *26* (1), 128–136.
(21) Su, Y.; Wei, H.; Li, T.; Geng, H.; Zhang, Y. *Mater. Res. Bull.* **2014**, *50*, 23–25.
(22) Gold nanoparticles - Biomedical Photonics, University of Gothenburg, Sweden http://cmb.gu.se/english/research/organic-and-medicinal-chemistry/Biomedical_Photonics/projects/gold-nanoparticles-/ (accessed Oct 6, 2015).
(23) Niidome, T.; Yamagata, M.; Okamoto, Y.; Akiyama, Y.; Takahashi, H.; Kawano, T.; Katayama, Y.; Niidome, Y. *J. Control. Release Off. J. Control. Release Soc.* **2006**, *114* (3), 343–347.
(24) Gupta, P.; Vermani, K.; Garg, S. *Drug Discov. Today* **2002**, *7* (10), 569–579.
(25) Peppas, N. A.; Keys, K. B.; Torres-Lugo, M.; Lowman, A. M. *J. Controlled Release* **1999**, *62* (1–2), 81–87.
(26) Esfand, R.; Tomalia, D. A. *Drug Discov. Today* **2001**, *6* (8), 427–436.
(27) Gillies, E. R.; Fréchet, J. M. J. *Drug Discov. Today* **2005**, *10* (1), 35–43.
(28) Kesharwani, P.; Jain, K.; Jain, N. K. *Prog. Polym. Sci.* **2014**, *39* (2), 268–307.

(29) Nanjwade, B. K.; Bechra, H. M.; Derkar, G. K.; Manvi, F. V.; Nanjwade, V. K. *Eur. J. Pharm. Sci.* **2009**, *38* (3), 185–196.
(30) Orive, G.; Anitua, E.; Pedraz, J. L.; Emerich, D. F. *Nat. Rev. Neurosci.* **2009**, *10* (9), 682–692.
(31) Roma-Rodrigues, C.; Raposo, L. R.; Cabral, R.; Paradinha, F.; Baptista, P. V.; Fernandes, A. R. *Int. J. Mol. Sci.* **2017**, *18* (1), 162.
(32) Zhuang Liu, J. T. R. *Mater. Today - MATER TODAY* **2011**, *14* (7), 316–323.
(33) Bamrungsap, S.; Zhao, Z.; Chen, T.; Wang, L.; Li, C.; Fu, T.; Tan, W. *Nanomed.* **2012**, *7* (8), 1253–1271.
(34) Goldstein, J. L.; Anderson, R. G. W.; Brown, M. S. *Nature* **1979**, *279* (5715), 679–685.
(35) Jayasena, S. D. *Clin. Chem.* **1999**, *45* (9), 1628–1650.
(36) Mullis, K. B.; Erlich, H. A.; Arnheim, N.; Horn, G. T.; Saiki, R. K.; Scharf, S. J. Process for amplifying, detecting, and/or-cloning nucleic acid sequences. US4683195 A, July 28, 1987.
(37) Oliphant, A. R.; Brandl, C. J.; Struhl, K. *Mol. Cell. Biol.* **1989**, *9* (7), 2944–2949.
(38) Stoltenburg, R.; Reinemann, C.; Strehlitz, B. *Biomol. Eng.* **2007**, *24* (4), 381–403.
(39) Eckert, K. A.; Kunkel, T. A. *Genome Res.* **1991**, *1* (1), 17–24.
(40) Liu, J.; Lu, Y. *Angew. Chem.* **2006**, *118* (1), 96–100.
(41) Song, S.; Wang, L.; Li, J.; Fan, C.; Zhao, J. *TrAC Trends Anal. Chem.* **2008**, *27* (2), 108–117.
(42) Bock, L. C.; Griffin, L. C.; Latham, J. A.; Vermaas, E. H.; Toole, J. J. *Nature* **1992**, *355* (6360), 564–566.
(43) Sefah, K.; Shangguan, D.; Xiong, X.; O'Donoghue, M. B.; Tan, W. *Nat. Protoc.* **2010**, *5* (6), 1169–1185.
(44) Barman, J. *RSC Adv* **2015**, *5* (16), 11724–11732.
(45) Zhang, Y.; Chen, Y.; Han, D.; Ocsoy, I.; Tan, W. *Bioanalysis* **2010**, *2* (5), 907–918.
(46) Orava, E. W.; Cicmil, N.; Gariépy, J. *Biochim. Biophys. Acta* **2010**, *1798* (12), 2190–2200.
(47) Zhang, J.; Chen, R.; Fang, X.; Chen, F.; Wang, Y.; Chen, M. *Nano Res.* **2015**, *8* (1), 201–218.
(48) Tan, W.; Fang, X. *Aptamers Selected by Cell-SELEX for Theranostics*; Springer, 2015.
(49) Jalalian, S. H.; Taghdisi, S. M.; Shahidi Hamedani, N.; Kalat, S. A. M.; Lavaee, P.; Zandkarimi, M.; Ghows, N.; Jaafari, M. R.; Naghibi, S.; Danesh, N. M.; Ramezani, M.; Abnous, K. *Eur. J. Pharm. Sci. Off. J. Eur. Fed. Pharm. Sci.* **2013**, *50* (2), 191–197.
(50) Dhar, S.; Gu, F. X.; Langer, R.; Farokhzad, O. C.; Lippard, S. J. *Proc. Natl. Acad. Sci.* **2008**, *105* (45), 17356–17361.
(51) Zhao, Z.; Xu, L.; Shi, X.; Tan, W.; Fang, X.; Shangguan, D. *Analyst* **2009**, *134* (9), 1808–1814.
(52) Wu, C.; Liu, J.; Zhang, P.; Li, J.; Ji, H.; Yang, X.; Wang, K. *Analyst* **2015**, *140* (17), 6100–6107.
(53) Rodrigues, A.; Emeje, M. *Carbohydr. Polym.* **2012**, *87* (2), 987–994.
(54) Bloembergen, S.; McLennan, I. J.; Jones, N.; WAGNER, R.; SHERMON, A. K. G.; ELSAYED, A. R.; Liu, J. Aptamer bioconjugate drug delivery device. US20120141551 A1, June 7, 2012.
(55) Bloembergen, S.; McLennan, I. J.; Jones, N.; Shermon, A. K. G.; Elsayed, A.; Liu, J. Aptamer bioconjugate drug delivery device. US20150025029 A1, January 22, 2015.

(56) Nutrition, C. for F. S. and A. Food Additives & Ingredients - High Fructose Corn Syrup: Questions and Answers http://www.fda.gov/Food/IngredientsPackagingLabeling/FoodAdditivesIngredients/ucm324856.htm (accessed Oct 6, 2015).
(57) Meshram, M. W.; Patil, V. V.; Mhaske, S. T.; Thorat, B. N. *Carbohydr. Polym.* **2009**, *75* (1), 71–78.
(58) Eloy, J. O.; Claro de Souza, M.; Petrilli, R.; Barcellos, J. P. A.; Lee, R. J.; Marchetti, J. M. *Colloids Surf. B Biointerfaces* **2014**, *123*, 345–363.
(59) Parnham, M. J.; Wetzig, H. *Chem. Phys. Lipids* **1993**, *64* (1), 263–274.
(60) Jun, Y. J.; Jadhav, V. B.; Min, J. H.; Cui, J. X.; Chae, S. W.; Choi, J. M.; Kim, I.-S.; Choi, S.-J.; Lee, H. J.; Sohn, Y. S. *Int. J. Pharm.* **2012**, *422* (1–2), 374–380.
(61) Woodhead, J. L.; Hall, C. K. *Macromolecules* **2011**, *44* (13), 5443–5451.
(62) Malecki, H. C.; Zupan, M. *Compos. Part Appl. Sci. Manuf.* **2012**, *43* (11), 1914–1920.
(63) Tagmatarchis, N. *Advances in Carbon Nanomaterials: Science and Applications*; CRC Press, 2012.
(64) Liu, R.; Sun, M.; Liu, X.; Fan, A.; Wang, Z.; Zhao, Y. *Int. J. Pharm.* **2014**, *462* (1–2), 103–107.
(65) Caminade, A.-M.; Turrin, C.-O.; Laurent, R.; Ouali, A.; Delavaux-Nicot, B. *Dendrimers: Towards Catalytic, Material and Biomedical Uses*; John Wiley & Sons, 2011.
(66) Mashkevich, B. O. *Drug Delivery Research Advances*; Nova Publishers, 2007.
(67) Narayanan, D.; Nair, S.; Menon, D. *Int. J. Biol. Macromol.* **2015**, *74*, 575–584.
(68) Santander, O. M. J.; Stauner, T.; Loretz, B.; Wenz, G.; Schaefer, U.; Lehr, C.-M. Starch nanoparticles for drug delivery systems. WO2010084088 A2, July 29, 2010.
(69) Corn Refiners Association. *Corn Starch*, 11th ed.; Corn Refiners Association: Washington, D.C.
(70) Moulay, S. *J. Polym. Eng.* **2013**, *33* (5), 389–443.
(71) Damager, I.; Engelsen, S. B.; Blennow, A.; Lindberg Møller, B.; Motawia, M. S. *Chem. Rev.* **2010**, *110* (4), 2049–2080.
(72) Wang, S.; Copeland, L. *Food Funct.* **2013**, *4* (11), 1564.
(73) Tetlow, I. J.; Emes, M. J. In *Comprehensive Biotechnology (Second Edition)*; Moo-Young, M., Ed.; Academic Press: Burlington, 2011; pp 37–45.
(74) Zobel, H. F. *Starch - Stärke* **1988**, *40* (1), 1–7.
(75) Xiao, H.-X.; Lin, Q.-L.; Liu, G.-Q.; Yu, F.-X. *Mol. Basel Switz.* **2012**, *17* (9), 10946–10957.
(76) Uslu, M.-K.; Polat, S. *Carbohydr. Polym.* **2012**, *87* (3), 1994–1999.
(77) S. LIM, P. A. S. *Cereal Chem* **1993**, *70* (2).
(78) Reddy, N.; Yang, Y. *Food Chem.* **2010**, *118* (3), 702–711.
(79) Shin, I.-S.; Park, N.-H.; Lee, J.-C.; Kim, K.-H.; Moon, C.; Kim, S.-H.; Shin, D.-H.; Park, S.-C.; Kim, H.-Y.; Kim, J.-C. *Drug Chem. Toxicol.* **2010**, *33* (3), 291–301.
(80) Bertolini, A. *Starches: Characterization, Properties, and Applications*; CRC Press, 2009.
(81) Sang, Y.; Prakash, O.; Seib, P. A. *Carbohydr. Polym.* **2007**, *67* (2), 201–212.
(82) Lack, S.; Dulong, V.; Picton, L.; Cerf, D. L.; Condamine, E. *Carbohydr. Res.* **2007**, *342* (7), 943–953.
(83) Rubens, R. W. Foodstuffs containing crosslinked starches using STMP. US4183969 A, January 15, 1980.
(84) Silva, M. C. *Ind. Crops Prod. 24* (1), 46–51.

(85) Le Corre, D.; Bras, J.; Dufresne, A. *Biomacromolecules* **2010**, *11* (5), 1139–1153.
(86) Mabey, W.; Mill, T. *J. Phys. Chem. Ref. Data* **1978**, *7* (2), 383–415.
(87) J. P. Robin; C. Mercier; R. Charbonniere; A. Guilbot. *Cereal Chem.* **1974**, *51*, 389–405.
(88) Jean-Luc Putaux, S. M.-B. *Biomacromolecules* **2003**, *4* (5), 1198–1202.
(89) Angellier, H.; Choisnard, L.; Molina-Boisseau, S.; Ozil, P.; Dufresne, A. *Biomacromolecules* **2004**, *5* (4), 1545–1551.
(90) Kim, J.-Y.; Yoon, J.-W.; Lim, S.-T. *Carbohydr. Polym.* **2009**, *78* (3), 626–632.
(91) Jong-Yea Kim, S.-T. L. *Carbohydr. Polym.* **2009**, *76* (1), 110–116.
(92) Bloembergen, S; Vanegdom, E; Wildi, R; Mclennan, I; Lee, D.I.; Klass, C.P.; Van Luewen, J. *J. Pulp Pap. Sci.* **2011**, *36* (3–4), 151–161.
(93) Lee, E. J.; Khan, S. A.; Lim, K.-H. *J. Biomater. Sci. Polym. Ed.* **2011**, *22* (4–6), 753–771.
(94) Tan, Y.; Xu, K.; Li, L.; Liu, C.; Song, C.; Wang, P. *ACS Appl. Mater. Interfaces* **2009**, *1* (4), 956–959.
(95) Chin, S. F.; Azman, A.; Pang, S. C.; Chin, S. F.; Azman, A.; Pang, S. C. *J. Nanomater. J. Nanomater.* **2014**, *2014*, *2014*, e763736.
(96) El-Naggar, M. E.; El-Rafie, M. H.; El-Sheikh, M. A.; El-Feky, G. S.; Hebeish, A. *Int. J. Biol. Macromol.* **2015**, *81*, 718–729.
(97) Bel Haaj, S.; Magnin, A.; Pétrier, C.; Boufi, S. *Carbohydr. Polym.* **2013**, *92* (2), 1625–1632.
(98) Shi, A.; Li, D.; Wang, L.; Li, B.; Adhikari, B. *Carbohydr. Polym.* **2011**, *83* (4), 1604–1610.
(99) Xiao, S.; Tong, C.; Liu, X.; Yu, D.; Liu, Q.; Xue, C.; Tang, D.; Zhao, L. *Chin. Sci. Bull.* **2006**, *51* (14), 1693–1697.
(100) Wildi, R. H.; Egdob, E. V.; Bloembergen, S. Process for producing biopolymer nanoparticles. US20110042841 A1, February 24, 2011.
(101) Tsai, T. H., *UWSpace*, **2015**.
(102) Wang, F.; Liu, J. *Nanoscale* **2013**, *5* (24), 12375–12382.
(103) Dave, N.; Liu, J. *ACS Nano* **2011**, *5* (2), 1304–1312.
(104) Gao, W.; Hu, C.-M. J.; Fang, R. H.; Zhang, L. *J. Mater. Chem. B* **2013**, *1* (48), 6569–6585.
(105) Gupta, A.; Eral, H. B.; Hatton, T. A.; Doyle, P. S. *Soft Matter* **2016**, *12* (11), 2826–2841.
(106) Friberg, S. E.; Corkery, R. W.; Blute, I. A. *J. Chem. Eng. Data* **2011**, *56* (12), 4282–4290.
(107) Van, S. J. J. G.; Stappers, F. H. M.; VAN, S. R. J. G.; Gottlieb, K. F.; Feil, H. Method for the preparation of starch particles. WO2000040617 A1, July 13, 2000.
(108) Greth, G. G.; Wilson, J. E. *J. Appl. Polym. Sci.* **1961**, *5* (14), 135–148.
(109) Sharma, K. S.; Patil, S. R.; Rakshit, A. K. *Colloids Surf. Physicochem. Eng. Asp.* **2003**, *219* (1–3), 67–74.
(110) Ee, S. L.; Duan, X.; Liew, J.; Nguyen, Q. D. *Chem. Eng. J.* **2008**, *140* (1–3), 626–631.
(111) Li, J.-L.; Bai, D.-S.; Chen, B.-H. *Colloids Surf. Physicochem. Eng. Asp.* **2009**, *346* (1–3), 237–243.
(112) Spernath, L.; Magdassi, S. *Polym. Adv. Technol.* **2007**, *18* (9), 705–711.
(113) Steven Bloembergen. (Personal Communication), 2016.
(114) Wu, Y.; Iglauer, S.; Shuler, P.; Tang, Y.; Goddard, W. A. *Tenside Surfactants Deterg.* **2010**, *47* (5), 280–287.

(115) Chuo, S. C.; Mohd-Setapar, S. H.; Mohamad-Aziz, S. N.; Starov, V. M. *Colloids Surf. Physicochem. Eng. Asp.* **2014**, *460*, 137–144.
(116) Berne, B. J.; Pecora, R. *Dynamic Light Scattering: With Applications to Chemistry, Biology, and Physics*; Courier Corporation, 1976.
(117) Pecora, R. *Dynamic Light Scattering: Applications of Photon Correlation Spectroscopy*; Springer Science & Business Media, 2013.
(118) Hunter, R. J. *Zeta Potential in Colloid Science: Principles and Applications*; Academic Press, 2013.
(119) Winey, M.; Meehl, J. B.; O'Toole, E. T.; Giddings, T. H. *Mol. Biol. Cell* **2014**, *25* (3), 319–323.
(120) Reimer, L. *Scanning Electron Microscopy: Physics of Image Formation and Microanalysis*; Springer Science & Business Media, 1998.
(121) Keeler, J. *Understanding NMR Spectroscopy*; John Wiley & Sons, 2011.
(122) Gorenstein, D. G. *Phosphorous-31 NMR: Principles and Applications*; Academic Press, 2012.
(123) Quin, L. D. *A Guide to Organophosphorus Chemistry*; John Wiley & Sons, 2000.
(124) Wong, R. S. H.; Ashton, M.; Dodou, K. *Pharmaceutics* **2015**, *7* (3), 305–319.
(125) Chavda, H.; Patel, C. *Int. J. Pharm. Investig.* **2011**, *1* (1), 17–21.
(126) Bueno, V. B.; Bentini, R.; Catalani, L. H.; Petri, D. F. S. *Carbohydr. Polym.* **2013**, *92* (2), 1091–1099.
(127) Nesrinne, S.; Djamel, A. *Arab. J. Chem.*
(128) Drozdov, A. D.; deClaville Christiansen, J. *Phys. Rev. E* **2015**, *91* (2), 22305.
(129) Cell Viability and Proliferation http://www.sigmaaldrich.com/technical-documents/articles/biofiles/cell-viability-and-proliferation.html (accessed Oct 6, 2015).
(130) *DrugBank*; DrugBank, Ed.; 2013.